## ORIGINAL RESEARCH

Pharmacologic Normalization of Pancreatic Cancer-Associated Fibroblast Secretome Impairs Prometastatic Cross-Talk With Macrophages

Rémi Samain,[1] Alexia Brunel,[1] Thibault Douché,[1] Marjorie Fanjul,[1] Stéphanie Cassant-Sourdy,[1] Julia Rochotte,[1] Jérôme Cros,[2] Cindy Neuzillet,[3] Jérôme Raffenne,[1] Camille Duluc,[1] Aurélie Perraud,[4] Jérémy Nigri,[5] Véronique Gigoux,[1] Ivan Bieche,[6] Matteo Ponzo,[7] Gilles Carpentier,[7] Ilaria Cascone,[7] Richard Tomasini,[5] Herbert A. Schmid,[8] Muriel Mathonnet,[4] Rémy Nicolle,[9] Marie-Pierre Bousquet,[10] Yvan Martineau,[1] Stéphane Pyronnet,[1] Christine Jean,[1] and Corinne Bousquet[1]

[1]Centre de Recherches en Cancérologie de Toulouse (CRCT), Université de Toulouse, INSERM Unité Mixte de Recherche UMR-1037, CNRS Equipe de Recherche Labellisée ERL5294, Equipe de Recherche Labellisée "Ligue Contre le Cancer" & "LabEx Toucan", Toulouse, France; [2]Department of Pathology, Beaujon-Bichat University Hospital–Paris Diderot University, Clichy, France; [3]Medical Oncology Department, Curie Institute, Versailles Saint-Quentin University, Saint Cloud, France; [4]Equipe d'Accueil EA 3842 Laboratory, Medicine and Pharmacy Faculties, University of Limoges, Limoges, France; [5]INSERM U1068/UMR 7258 CNRS, Cancer Research Center of Marseille, Marseille, France; [6]Department of Genetics, Institut Curie, Paris Descartes University, Paris, France; [7]Growth, Reparation and Tissue Regeneration Laboratory, Equipe de Recherche Labellisée ERL-CNRS 9215, University of Paris-Est, Créteil, France; [8]Novartis Pharmaceuticals, Basel, Switzerland; [9]Programme Cartes d'Identité des Tumeurs, Ligue Nationale Contre Le Cancer, Paris, France; [10]Institute for Pharmacology and Structural Biology, University of Toulouse, Toulouse, France
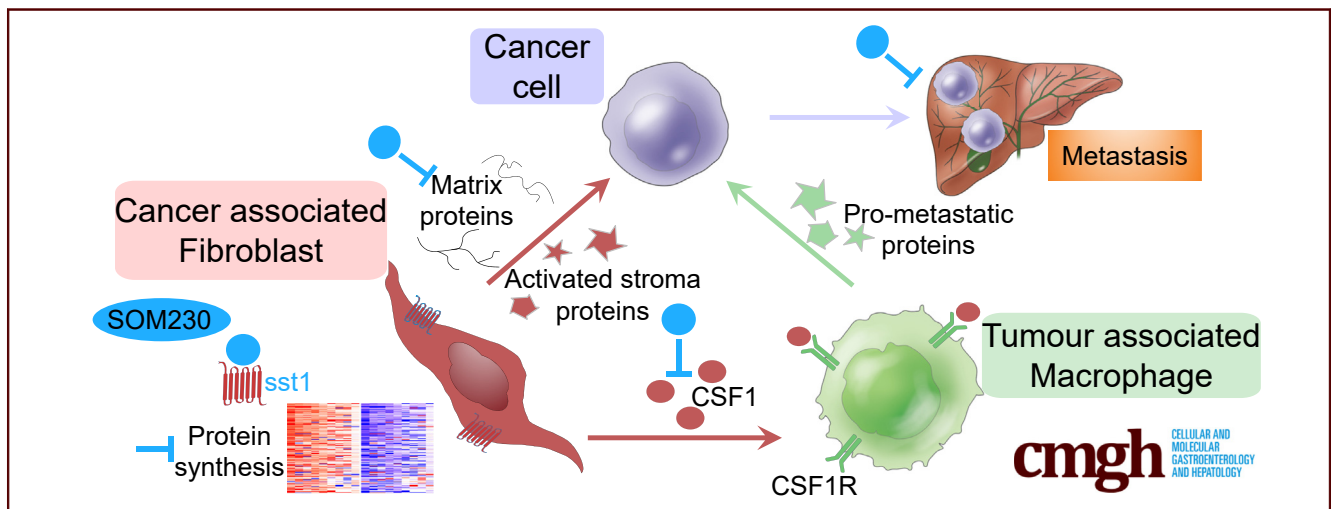
SUMMARY

Cancer-associated fibroblasts orchestrate pancreatic adenocarcinoma (PDA) aggressiveness. We show that the Food and Drug Administration–approved somatostatin analog SOM230 inhibits metastasis in murine PDA models by acting through its receptor sst1 to disrupt the cancer-associated fibroblast production of colony stimulating factor 1, a prometastatic and macrophage-attracting chemokine whose stromal expression is associated with PDA aggressiveness.

BACKGROUND & AIMS: Cancer-associated fibroblasts (CAFs) from pancreatic adenocarcinoma (PDA) present high protein synthesis rates. CAFs express the G-protein–coupled somatostatin receptor sst1. The sst1 agonist SOM230 blocks CAF protumoral features in vitro and in immunocompromised mice. We have explored here the therapeutic potential of SOM230, and underlying mechanisms, in immunocompetent models of murine PDA mimicking the heavy fibrotic and immunosuppressive stroma observed in patient tumors.

METHODS: Large-scale mass spectrometry analyses were performed on media conditioned from 9 patient PDA-derived CAF primary cultures. Spontaneous transgenic and experimental (orthotopic co-graft of tumor cells plus CAFs) PDA-bearing mice were longitudinally ultrasound-monitored for tumor and metastatic progression. Histopathology and flow cytometry analyses were performed on primary tumors and metastases. Stromal signatures were functionally validated through bioinformatics using several published, and 1 original, PDA database.

RESULTS: Proteomics on the CAF secretome showed that SOM230 controls stromal activities including inflammatory responses. Among the identified secreted proteins, we validated that colony-stimulating factor 1 (CSF-1) (a macrophage growth factor) was reduced by SOM230 in the tumor and plasma of PDA-harboring mice, alongside intratumor stromal normalization (reduced CAF and macrophage activities), and dramatic metastasis reduction. In transgenic mice, these SOM230 benefits alleviate the chemotherapy-induced (gemcitabine) immunosuppressive stroma reshaping. Mechanistically, SOM230 acts in vivo on CAFs through sst1 to disrupt prometastatic CAF production of CSF-1 and cross-talk with macrophages. We found that in patients, stromal CSF-1 was associated with aggressive PDA forms.

CONCLUSIONS: We propose SOM230 as an antimetastatic therapy in PDA for its capacity to remodel the fibrotic and immunosuppressive myeloid stroma. This pharmacotherapy should benefit PDA patients treated with chemotherapies. *(Cell Mol Gastroenterol Hepatol 2021;11:1405–1436; https://doi.org/10.1016/j.jcmgh.2021.01.008)*

Pancreatic ductal adenocarcinoma (PDA) remains one of the deadliest neoplasms. Most patients die from metastatic disease within the first year after diagnosis.[1] Stratifying PDA tumors using genetic profiles has not proven to be valuable for predicting therapeutic responses and clinical outcome in PDA, whereas transcriptomic profiles have defined 2 tumor subgroups in relation to tumor aggressiveness.[2,3] Molecular profiles of the tumor and stromal compartments are reported to be of prognostic value.[4–6] Consistently, a cross-talk between tumor cells and their stroma now is recognized as being critically involved in PDA progression and resistance to treatments.[7] Hence, PDA tumors are characterized by a prominent desmoplastic reaction, which represents up to 80% of the tumor mass and comprises acellular organized matrix fibers produced mainly by activated fibroblasts within the tumor, termed *cancer-associated fibroblasts* (CAFs). CAFs are the most abundant cells in PDA stroma, and secrete, in addition to extracellular matrices, growth and angiogenic factors, as well as cytokines and chemokines, which favor tumor progression and chemoresistance.[8] Immaturity of PDA stroma, linked with a high stromal cell content, correlates with a poor prognosis, emphasizing the critical role of stromal cells in dictating tumor cell behavior.[9] In addition to CAFs, PDA stroma comprise immune cells, mostly tumor-associated macrophages (TAMs) of myeloid origin and polarized to an M2 phenotype with immunosuppressive activities. By secreting extracellular matrix remodeling enzymes; growth, angiogenic, and redox factors; and cytokines, this myeloid subset dampens antitumoral immune reactions and facilitates tumor cell invasion and metastasis.[10,11] In vitro studies also showed that pancreatic CAFs induce monocyte polarization into immunosuppressive M2-like macrophages,[12]

suggesting that a dynamic cross-talk exists between these stromal cells, impacting tumor cell biology. Thus, PDA stroma plays a prominent role in its aggressiveness and resistance to therapy, yet remains difficult to target owing to its cellular and functional heterogeneity.[13,14] The use of murine models mimicking the complex interactions between pancreatic cancer cells and their microenvironment offers research opportunities in a therapeutic perspective. Using in vitro settings and an immunocompromised mouse model of PDA, our previous work has shown that protein synthesis dependent on the Akt-mechanistic Target Of Rapamycin (mTOR) pathway is abnormally activated in primary cultures of CAFs compared with nonactivated pancreatic stellate cells (PSCs) (isolated from healthy pancreas), and is required for the promotion of pancreatic tumor cell metastasis and chemoprotection.[15,16] Hence, pharmacologic inhibition of this pathway in CAFs abrogates the translation of messenger RNA (mRNA) encoding the secreted protein interleukin 6, directly impacting tumor cell epithelial-to-mesenchymal transition and chemoresistance.[15,16] Inhibition of the Akt-mTOR pathway was achieved using the somatostatin analog SOM230 (Pasireotide; Novartis, Basel, Switzerland) targeting the somatostatin G-protein–coupled receptor subtype 1 (GPCR) sst1, which we identified to be expressed in CAFs but not in PSCs,[15,16] as later confirmed by others.[17]

Here, we aimed at exhaustively uncovering the impact of SOM230 on CAFs to identify mechanisms for its putative therapeutic benefit in relevant immunocompetent murine models of experimental and spontaneous PDA.[18] Large-scale, mass-spectrometry (MS) analyses of the secretome of 9 patient tumor-derived CAF primary cultures showed SOM230-inhibited proteins enriched in published PDA "stroma-activated" signatures,[4,6] and involved in inflammatory responses. Accordingly, SOM230 showed antimetastatic activity in relevant PDA-harboring mice, normalizing the fibrotic and immunosuppressive myeloid stroma, including the cytokinic storm reaction induced by chemotherapy (gemcitabine).[19] Mechanistically, SOM230 acts through the CAF-expressed sst1 receptor to disrupt a prometastatic cross-talk between CAFs and immunosuppressive TAMs involving the chemokine colony-stimulating factor (CSF-1),

Most current article

whose specific expression in the stroma of patient tumors was found to be associated with aggressive and metastatic forms of PDA.

Results

SOM230 Decreases CAF Production of Secreted Proteins Enriched in PDA Stroma-Activated Signatures

To exhaustively identify CAF-secreted proteins, we performed MS analyses on media conditioned by 9 CAF explants, treated or not with SOM230 for 48 hours (Figure 1A). A total of 272 proteins were identified as being significantly ($P < .05$) down-regulated (threshold of 2-fold) by SOM230, but none were up-regulated (Figure 1B, Table 1). These proteins are graphically represented for each CAF in heatmaps with box plots for global levels (Figure 1C), and averaged in the secretomes of the 9 CAF cultures (Figure 1D) where pairs between SOM230-treated and control untreated conditions are indicated. Gene set enrichment analysis (GSEA) for this SOM230-regulated secretomic signature identified pathways including Phosphoinositide 3-kinase (PI3K–AKT) and mTOR signalings and the inflammatory response pathway (Figure 1E). Among the 272 identified proteins, 75 and 54 were common to the "stroma-activated" signature from Moffitt et al,[4] or from Puleo et al,[6] respectively (Figure 1F), with a significant normalized enrichment score (Figure 1G), and 47 proteins were common to both signatures (listed in Figure 1F). Dependency on sst1 expression of several of the identified SOM230-regulated secretomic signatures (biglycan, connective tissue growth factor, and thrombospondin 2 in Table 1) was confirmed in human CAFs knocked-down for sst1 (Figure 1H). These results suggest that SOM230 normalizes numerous cross-talks originating from sst1-expressing CAFs, putatively regulating both tumor cells and stromal biology.

SOM230 Reduces Metastasis in PDA Mouse Models Through the GPCR sst1 Expressed on CAFs
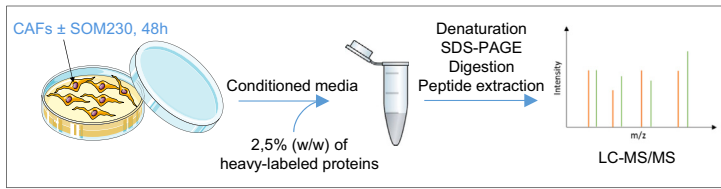
We previously showed that SOM230 is antimetastatic in immunocompromised mice, by indirectly, through its action on CAFs, inhibiting epithelial-to-mesenchymal transition in PDA tumor cells.[16] To evaluate whether SOM230 normalized the PDA stroma in models closer to the clinic, we developed an immunocompetent murine model consisting of the orthotopic co-graft of syngeneic C57BL/6 tumor cells (derived from *Pdx-1-Cre; LSL-Kras*$^{G12D/+}$*; LSL-Trp53*$^{R172H/+}$ tumors [KPC tumors]),[18] with PSCs isolated from either wild-type (WT) or sst1 knock-out (KOsst1) C57BL/6 mouse pancreata[20] (Figure 2A and B). First, these PSCs were characterized phenotypically. Ex vivo–grown WT mice PSCs were activated (as attested by up-regulation of α smooth muscle actin [αSMA] expression) and spontaneously acquired the expression of GPCR sst1 (Figure 2C). They also presented high protein synthesis rates (monitored by surface sensing of translation [SUnSET]),[21] as we

previously published in human CAFs,[15] these rates were reduced by SOM230, as was the expression of the extracellular matrix (ECM) protein and CAF marker periostin (Figure 2D).[22] Accordingly, periostin was identified in the SOM230-regulated, patient-derived CAF secretomic signature (Table 1). KOsst1 mice PSCs showed equivalent high intrinsic protein synthesis rates and periostin expression as WT PSCs, but were not responsive to SOM230 treatment (Figure 2D). WT or KOsst1 PSCs then were co-grafted with tumor cells in C57BL/6 mice, which were later treated or not with SOM230 once tumors were formed, as indicated (Figure 2E). No SOM230 effect was observed on primary tumor growth in any group (Figure 2F), whereas the drug significantly reduced lung metastasis incidence and tumor load (defined as the cumulative lung metastatic area, less than or more than 0.1% of the total lung area) in mice co-grafted with tumor cells and WT PSCs (Figure 2G and H). No liver metastases were observed in this model. SOM230 did not significantly inhibit metastasis in mice co-grafted with KOsst1 PSCs. Altogether, these results show that SOM230 is antimetastatic in a novel immunocompetent PDA model because of its action on sst1 expressed by CAFs.
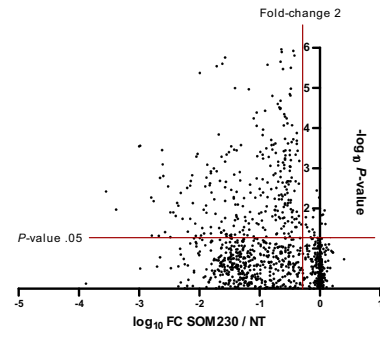
SOM230 Inhibits Metastasis by Decreasing CAF-Secreted CSF-1

To identify CAF-secreted proteins involved in the drug antimetastatic effect, we searched for factors down-regulated by SOM230 both in the CAF secretome (Table 1) and in the plasma of mice grafted with KPC tumor cells plus PSCs and treated with SOM230 (from Figure 2) (Figure 3A and B, Table 2). Five common proteins were identified (Figure 3C), including periostin and the chemokine CSF-1.[4] We focused on CAF-secreted CSF-1. We confirmed by enzyme-linked immunosorbent assay (ELISA) that SOM230 decreased CSF-1 in patient CAF-conditioned media (Figure 3D). Importantly, we found that sst1-expressing CAFs also co-expressed CSF-1, as assessed by confocal immunofluorescence imaging of patient PDA tissues (Figure 3E). In the plasma of grafted and SOM230-treated mice (from Figure 2), we confirmed that SOM230 decreased the CSF-1 concentration in a dependent manner to CAF-expressed sst1 (Figure 3F). CSF-1 expression also was reduced by SOM230 in the primary tumors of treated mice (Figure 3G) (the different 50- to 60-kilodalton-weight bands visualized by Western blot are consistent with the described spliced and matured forms of CSF-1).[23] To test the role of CAF-secreted CSF-1 on the antimetastatic effect of SOM230, KPC tumor cells then were co-grafted in the pancreas of syngeneic mice with WT or CSF-1–overproducing and secreting PSCs (CSF-1 PSCs). We confirmed by ELISA a high CSF-1 production in conditioned media of CSF-1 PSCs (122 ± 5 ng/mL), which SOM230 was unable to reduce (Figure 3H). Upon orthotopic co-graft in C57BL/6 mice of tumor cells with WT or CSF-1 PSCs, no significant difference in tumor growth or in metastatic potential was observed in the untreated condition, and SOM230 did not impact primary tumor growth in WT PSCs or in CSF-1–transduced PSCs (Figure 3I and J). However, the
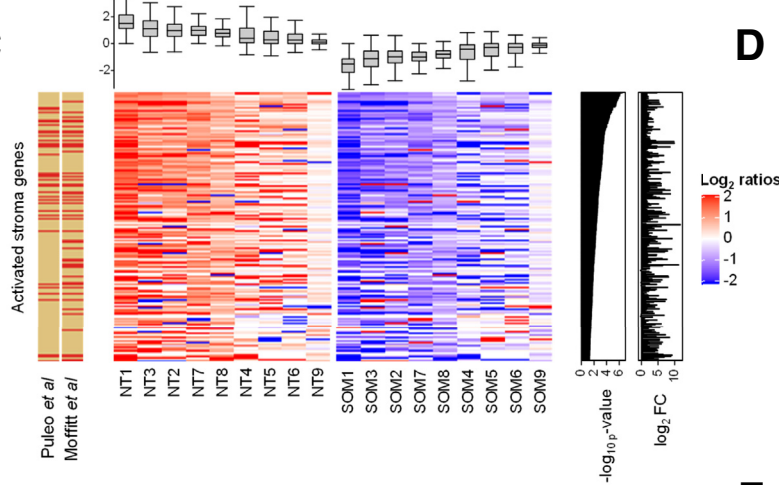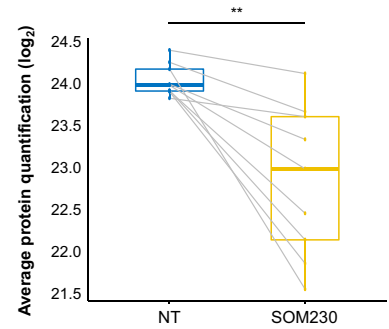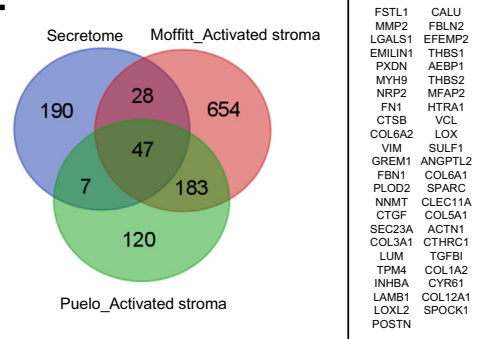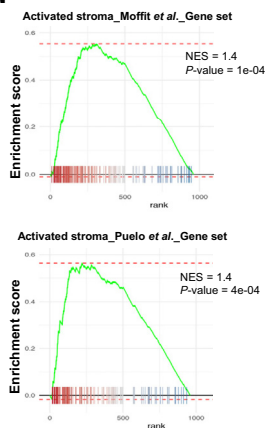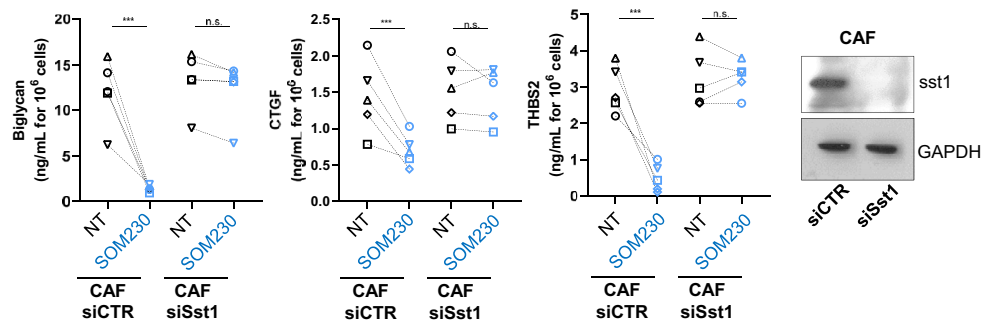
expected SOM230 inhibitory effect on lung metastasis incidence and load observed with WT PSCs was abrogated when PSCs overexpressed secreted CSF-1 (Figure 3J and K). These results show the critical role of CAF-derived CSF-1 in the antimetastatic effect of SOM230.

SOM230, Acting Through the CAF-Expressed GPCR sst1, Normalizes the Inflammatory PDA Stroma

Because the CSF-1 chemokine is involved in monocyte recruitment and activation,[24] we performed fluorescence-activated cell sorter analysis on pancreatic tumors grown in mice co-grafted with tumor cells plus WT or KOsst1 PSCs (Figure 4A and B). SOM230 treatment did not significantly impact intratumor load of total CD45, but decreased that of F4/80$^+$ macrophages, and of the F4/80$^+$CD11b$^+$CD206$^+$ macrophage subset, whereas the CD11b$^+$Gr1$^+$ subset myeloid-derived suppressor cell was not affected (Figure 4C–F). In contrast, no significant effect of SOM230 on macrophage subsets was observed when KOsst1 PSCs were co-grafted (Figure 4D–F). SOM230 treatment did not impact the proportions of CD3$^+$, CD4$^+$, and CD8$^+$ lymphoid cell populations (Figure 4G–I). These results indicate that SOM230 decreases the intratumor macrophage load, including the F4/80$^+$CD11b$^+$CD206$^+$ subset comprising TAMs.

SOM230 Is Antimetastatic in a Murine Spontaneous Model of PDA

The therapeutic and stroma-normalizing benefits of SOM230 were tested in KPC mice, developing a spontaneous PDA recognized to closely mimic the human pathology and its fibrotic immune stroma.[18] We showed by immunohistochemistry that sst1 was expressed in the αSMA-positive KPC tumor stroma (Figure 5A). Because all PDA patients receive chemotherapy and to get closest to clinical reality, SOM230 treatment of KPC mice also was evaluated in a chemotherapy background (gemcitabine), as indicated (Figure 5B), starting at equal ultrasound-calculated mean volumes between treatment groups (Figure 5C). We observed that tumor volume progression, which was exponential from day 1 to 21 in untreated mice, was reduced significantly in the combination-treated group (gemcitabine plus SOM230), but not by gemcitabine or SOM230 alone (Figure 5D–H). The combination therapy also significantly reduced tumor growth and extended survival, compared with untreated or gemcitabine-treated mice, in another spontaneous transgenic mouse PDA model (Pdx1-Cre; LSL-Kras^{G12D}; Ink4a$^{fl/fl}$), in which gemcitabine alone also was efficient (Figure 5I). In KPC mice, metastatic incidence and load were analyzed in the liver (only rare lung micrometric metastases were visualized). This was comparatively quantified in KPC mice presenting equivalent primary tumor volume after killing (Table 3), to avoid the evaluation of a drug antimetastatic potential directly linked to its delaying effect on primary tumor growth. The combination therapy significantly reduced liver metastatic incidence and load because only 4 of 8 mice in this group presented liver metastases with a low metastatic load (defined as <3% of cumulative liver metastatic area), against 7 of 8 in the untreated or gemcitabine-treated group, which presented in most cases a high metastatic load (Figure 5K and L). In contrast, SOM230 did not have an antimetastatic effect when administered alone, although 2 of 8 SOM230-treated mice, whose tumor growth was delayed by SOM230 (mice number 734 and 1027) (Figure 5G, Table 3), also were nonmetastatic. Only the combination therapy significantly extended mouse survival, as compared with no treatment (Figure 5M). These results show that SOM230 is inefficient to inhibit metastatic spread in KPC mice when used alone, but is antimetastatic in a gemcitabine-treated background.

Immunopathology of KPC primary tumors showed that SOM230 treatment, when combined with chemotherapy, did not increase the cytotoxicity of gemcitabine, which

---

Figure 1. (*See previous page*). **SOM230 decreases CAF production of secreted proteins enriched in PDA activated stroma signatures.** (*A*) Experimental design of CAF secretome analysis. (*B*) Graphic representation of quantitative proteomics data. Proteins are ranked in a volcano plot according to their statistical *P* value (y-axis) and their relative abundance ratio (log fold change) between untreated (NT) and SOM230-treated CAFs (x-axis). (*C*) SOM230-modulated protein secretion. Heatmap showing the differentially secreted proteins in 9 CAF cultures treated (SOM) or not (NT) with SOM230. Proteins are ordered by the level of significance of the differential test. The first 2 columns indicate if each protein was associated previously with an activated form of stroma in human primary tumors (Moffit et al[4] or Puleo et al[6] databases). The 2 main heatmaps show the level of quantification, normalized by pairs of treated/untreated CAFs as log^2 ratios, in each experiment. *Upper box plots* show the global levels of these differentially secreted proteins. The 2 right panels illustrate the *P* value of the differential analysis and the log fold change (FC). (*D*) Box plot of the average of all secreted protein quantification measured in each sample. Pairs between SOM230-treated and untreated conditions are indicated by a gray segment. The Wilcoxon matched-pairs signed rank test was used to generate *P* values. **$P < .01$. (*E*) Gene set enrichment analysis for down-regulated pathways in SOM230-treated CAF secretomes, as compared with untreated CAFs. (*F*) Venn diagram of the overlap of down-regulated proteins in secretome analysis and activated stroma signatures from the Moffitt et al[4] or Puleo et al[6] databases. Common proteins are listed in the *right panel*. (*G*) Gene set enrichment analysis comparing secretome genes and activated stroma signatures from Moffitt et al[4] and Puleo et al.[6] (*H*) CAF primary cultures (n = 5) were transfected with a small interfering RNA targeting sst1 (siSst1) or a control nontargeting siRNA (siCTR), and treated or not (NT) with SOM230. Biglycan, connective tissue growth factor (CTGF), and thrombospondin (THBS 2) were quantified in the CAF conditioned media by ELISA (n = 5, Kruskal–Wallis test followed with the Dunn multiple comparison post-test was used to generate *P* values, ***$P < .001$). Representative Western blot showing expression of sst1 and glyceraldehyde-3-phosphate dehydrogenase (GAPDH) (internal loading control for protein expression in each condition) in CAFs. LC, liquid chromatography; NES, normalized enriched score; SDS-PAGE, sodium dodecyl sulfate–polyacrylamide gel electrophoresis.

Table 1. Listing of Significantly Down-Regulated Proteins in CAF's Secretome: Untreated Vs SOM230

Protein names	Gene names	Moy ratio NT/SOM230	P value
Decorin	DCN	3565.20	.0037699
Biglycan	BGN	2416.98	.0105944
Thrombospondin-2	THBS2	993.52	.0002836
Glia-derived nexin	SERPINE2	944.33	.0002733
Adipocyte enhancer-binding protein 1	AEBP1	629.64	.0053412
Agrin	AGRN	618.31	.0478032
Fibulin-1	FBLN1	572.34	.0065804
Peroxidasin homolog	PXDN	468.76	.0481937
Carboxypeptidase E	CPE	448.97	.0017332
HLA class I histocompatibility antigen	HLA-A	412.95	.0003536
Protein-lysine 6-oxidase	LOX	405.09	.0007965
Elongation factor 1-δ	EEF1D	401.99	.0015514
Stromelysin-1	MMP3	369.77	.0387783
SPARC	SPARC	334.84	.0028440
Glyceraldehyde-3-phosphate dehydrogenase, testis-specific	GAPDHS	302.95	.0125467
Coiled-coil domain-containing protein 80	CCDC80	269.82	.0124452
Calumenin	CALU	244.86	.0154646
Out at first protein homolog	OAF	232.27	.0072591
Fibrillin-1	FBN1	223.43	.0085725
Testican-1	SPOCK1	202.29	.0041202
Connective tissue growth factor	CTGF	189.63	.0180345
Fibulin-2	FBLN2	160.13	.0030805
Collagen α-1(V) chain	COL5A1	153.20	.0376581
Syndecan-4	SDC4	142.77	.0181431
Phospholipid transfer protein	PLTP	140.32	.0027074
A disintegrin and metalloproteinase with thrombospondin motifs 1	ADAMTS1	139.38	.0020889
Sushi repeat-containing protein SRPX2	SRPX2	131.96	.0014868
Complement C1r subcomponent	C1R	129.50	.0073546
Sushi repeat-containing protein SRPX	SRPX	116.75	.0239367
Vitamin K–dependent protein S	PROS1	115.14	.0483223
Actin, cytoplasmic 1; actin, cytoplasmic 1, N-terminally processed	ACTB	112.36	.0005106
Plasma α-L-fucosidase	FUCA2	108.05	.0004376
Laminin subunit γ-1	LAMC1	97.78	.0000042
Inhibin β A chain	INHBA	93.39	.0471213
Proliferating cell nuclear antigen	PCNA	89.42	.0306750
Stanniocalcin-2	STC2	84.81	.0108231
Tumor necrosis factor–receptor superfamily member 11B	TNFRSF11B	82.61	.0418658
Tryptophan–transfer RNA ligase	WARS	79.58	.0028410
Latent-transforming growth factor β-binding protein 1	LTBP1	78.27	.0084952
Myosin-14	MYH14	76.43	.0017097
Gelsolin	GSN	76.16	.0128688
Latent-transforming growth factor β-binding protein 2	LTBP2	74.59	.0008218
Netrin-4	NTN4	67.79	.0026525
Protein transport protein Sec23A	SEC23A	65.55	.0023638
Coagulation factor IX	F9	64.96	.0289241
Septin-7	SEPT-7	64.92	.0419335
Microfibrillar-associated protein 2	MFAP2	64.75	.0011975
Collagen α-2(I) chain	COL1A2	64.69	.0013190
Serine protease HTRA1	HTRA1	62.57	.0039875

Table 1. Continued

Protein names	Gene names	Moy ratio NT/SOM230	P value
Collagen α-1(III) chain	COL3A1	57.28	.0010022
γ-enolase	ENO2	56.15	.0059011
Tripeptidyl-peptidase 1	TPP1	53.61	.0135799
β-hexosaminidase subunit β	HEXB	51.51	.0000029
T-complex protein 1 subunit γ	CCT3	51.00	.0011871
Amyloid-like protein 2	APLP2	48.18	.0001436
Urotensin-2	UTS2	47.26	.0307781
60S acidic ribosomal protein P1	RPLP1	45.66	.0020590
Angiopoietin-related protein 2	ANGPTL2	43.54	.0396281
Nascent polypeptide-associated complex subunit α	NACA	43.35	.0397871
Complement C1s subcomponent	C1S	43.01	.0212752
Glutathione S-transferase P	GSTP1	42.75	.0005148
Calsyntenin-1; soluble Alc-α; CTF1-α	CLSTN1	41.57	.0000025
Ras-related protein Rab-6A	RAB6A	38.84	.0354047
Proactivator polypeptide; saposin-A	PSAP	37.12	.0000017
Dickkopf-related protein 3	DKK3	37.04	.0064695
F-actin-capping protein subunit β	CAPZB	36.85	.0006800
Tubulin α-4A chain	TUBA4A	36.76	.0029517
Clathrin heavy chain 1	CLTC	36.73	.0172379
Deoxyuridine 5-triphosphate nucleotidohydrolase, mitochondrial	DUT	36.34	.0021730
Proteasome subunit β type-6	PSMB6	35.95	.0444021
Proprotein convertase subtilisin/kexin type 9	PCSK9	35.87	.0432914
72-kilodalton type IV collagenase; PEX	MMP2	35.79	.0004569
Prolyl 3-hydroxylase 1	LEPRE1	35.26	.0496856
Lactadherin; lactadherin short form; medin	MFGE8	32.58	.0003940
Elongation factor 1-γ	EEF1G	31.24	.0469751
Ferritin light chain	FTL	29.77	.0450262
Lupus La protein	SSB	29.38	.0002821
Follistatin-related protein 5	FSTL5	29.37	.0034505
Matrix-remodeling-associated protein 5	MXRA5	27.17	.0056534
Eukaryotic initiation factor 4A-II	EIF4A2	27.13	.0271990
WD repeat-containing protein 65	WDR65	27.05	.0052157
Extracellular sulfatase Sulf-1	SULF1	26.38	.0003432
Calponin-3	CNN3	26.17	.0014325
Protein phosphatase 2 scaffold subunit α	PPP2R1A	25.84	.0446915
β-1,4-galactosyltransferase 5	B4GALT5	25.78	.0196639
Serum albumin	ALB	25.68	.0000003
Synaptic vesicle membrane protein VAT-1 homolog	VAT1	25.46	.0000100
Splicing factor, proline- and glutamine-rich	SFPQ	24.92	.0079895
Glucose-6-phosphate 1-dehydrogenase	G6PD	24.56	.0146303
Cochlin	COCH	24.14	.0038765
Platelet-activating factor acetylhydrolase IB subunit α	PAFAH1B1	23.88	.0003566
Extracellular matrix protein 1	ECM1	23.79	.0160787
Vacuolar protein sorting-associated protein 35	VPS35	23.12	.0179969
Exostosin-1	EXT1	22.83	.0080334
Protein S100-A6	S100A6	21.49	.0386695
Neutral α-glucosidase AB	GANAB	21.27	.0012394
Podocan	PODN	20.85	.0020030
Fascin	FSCN1	20.41	.0002658

Table 1. Continued

Protein names	Gene names	Moy ratio NT/SOM230	P value
Olfactomedin-like protein 3	OLFML3	19.10	.0087429
T-complex protein 1 subunit η	CCT7	19.08	.0349927
Membrane-bound transcription factor site-1 protease	MBTPS1	18.28	.0444638
Procollagen-lysine, 2-oxoglutarate 5-dioxygenase 3	PLOD3	18.25	.0290330
Heterogeneous nuclear ribonucleoprotein K	HNRNPK	18.10	.0055013
Peroxiredoxin-4	PRDX4	17.52	.0163462
Heat shock protein 75 kilodaltons, mitochondrial	TRAP1	16.80	.0203181
ANK repeat and PH domain-containing protein 1	ACAP1	15.73	.0465981
Clusterin; clusterin β chain; clusterin α chain	CLU	15.19	.0000107
Macrophage colony-stimulating factor 1	CSF1	15.06	.0234921
EMILIN-1	EMILIN1	14.74	.0335435
Low-density lipoprotein receptor	LDLR	14.45	.0122306
Laminin subunit β-2	LAMB2	14.41	.0025413
Carbonyl reductase [reduced nicotinamide adenine dinucleotide phosphate] 3	CBR3	14.29	.0040576
Serpin B6	SERPINB6	13.24	.0184994
60-kilodalton heat shock protein, mitochondrial	HSPD1	12.71	.0000572
Adenosine triphosphate-citrate synthase	ACLY	12.46	.0495593
Glypican-1; secreted glypican-1	GPC1	11.88	.0054106
Periostin	POSTN	11.34	.0000412
45-kilodalton calcium-binding protein	SDF4	11.31	.0000878
Importin-5	IPO5	11.24	.0232329
Inositol monophosphatase 1	IMPA1	11.10	.0017802
Fibulin-5	FBLN5	11.09	.0004997
Collagen triple-helix repeat-containing protein 1	CTHRC1	10.55	.0246140
Glutathione S-transferase Ω-1	GSTO1	10.24	.0134160
β-2-microglobulin	B2M	9.94	.0032569
Actin-related protein 3	ACTR3	9.67	.0003930
Transcriptional activator protein Pur-β	PURB	9.53	.0046924
Elongation factor 1-β	EEF1B2	9.41	.0125778
Protein phosphatase 1 regulatory subunit 12A	PPP1R12A	9.11	.0201546
Nucleobindin-2	NUCB2	8.99	.0004586
Fibronectin	FN1	8.92	.0001491
Collagen α-2(VI) chain	COL6A2	8.87	.0018644
6-phosphogluconate dehydrogenase, decarboxylating	PGD	8.79	.0040032
Amyloid β A4 protein	APP	8.77	.0005750
Transferrin-receptor protein 1	TFRC	8.65	.0001086
Annexin A2	ANXA2	8.64	.0301342
Elongation factor 2	EEF2	8.11	.0000368
Acetyl-CoA acetyltransferase, cytosolic	ACAT2	8.05	.0340549
α-soluble NSF (attachment protein	NAPA	7.90	.0118155
Epidermal growth factor–containing fibulin-like extracellular matrix protein 2	EFEMP2	7.84	.0003193
Heat shock 70-kilodalton protein 1A/1B	HSPA1A	7.64	.0088805
Ubiquitin-like modifier-activating enzyme 1	UBA1	7.44	.0052055
Talin-1	TLN1	7.41	.0000026
Tropomyosin α-3 chain	TPM3	7.41	.0022479
Nucleophosmin	NPM1	7.14	.0005244
Thrombospondin-1	THBS1	6.59	.0008619
β-hexosaminidase subunit α	HEXA	6.47	.0001968

Table 1. Continued

Protein names	Gene names	Moy ratio NT/SOM230	*P* value
Cysteine–transfer RNA ligase, cytoplasmic	*CARS*	6.47	.0033002
C-type lectin domain family 11 member A	*CLEC11A*	6.34	.0002634
Cysteine and glycine-rich protein 1	*CSRP1*	6.23	.0157997
Galectin-3-binding protein	*LGALS3BP*	6.20	.0003411
Nucleobindin-1	*NUCB1*	6.19	.0000158
Proteasome subunit β type-4	*PSMB4*	5.86	.0014785
Follistatin-related protein 1	*FSTL1*	5.86	.0002589
Ras guanosine triphosphatase-activating-like protein IQGAP1 (IQ Motif Containing GTPase Activating Protein 1)	*IQGAP1*	5.68	.0108885
Ribonuclease inhibitor	*RNH1*	5.63	.0057533
Actin, α cardiac muscle 1	*ACTC1*	5.55	.0002417
Cathepsin B	*CTSB*	5.53	.0145813
Protein disulfide-isomerase A4	*PDIA4*	5.51	.0109743
Myosin light polypeptide 6	*MYL6*	5.45	.0013450
Serine/threonine-protein phosphatase 1 (PP1)-β catalytic subunit	*PPP1CB*	5.36	.0194514
Hsp90 co-chaperone Cdc37	*CDC37*	5.34	.0088745
Transforming growth factor-β–induced protein ig-h3	*TGFBI*	5.33	.0004158
Purine nucleoside phosphorylase	*PNP*	5.26	.0437861
Collagen α-1(XII) chain	*COL12A1*	5.22	.0030738
T-complex protein 1 subunit θ	*CCT8*	5.14	.0419163
Peroxiredoxin-2	*PRDX2*	5.03	.0113992
Epidermal growth factor–containing fibulin-like extracellular matrix protein 1	*EFEMP1*	5.00	.0000249
Nucleosome assembly protein 1-like 4	*NAP1L4*	4.88	.0008493
Myosin-9	*MYH9*	4.88	.0021392
Tubulin β chain	*TUBB*	4.85	.0006886
Hsc70-interacting protein	*ST13*	4.81	.0047255
Importin subunit α-3	*KPNA4*	4.81	.0059251
Sulfhydryl oxidase 1	*QSOX1*	4.74	.0163887
Tubulin β-4B chain	*TUBB4B*	4.68	.0000303
Nidogen-1	*NID1*	4.58	.0176328
Cathepsin D	*CTSD*	4.57	.0000334
Adenylyl cyclase-associated protein 1	*CAP1*	4.51	.0000022
Importin subunit β-1	*KPNB1*	4.51	.0011822
Laminin subunit β-1	*LAMB1*	4.46	.0016507
WD repeat-containing protein 1	*WDR1*	4.45	.0000318
Tubulin α-1B chain	*TUBA1B*	4.43	.0000209
Aspartate aminotransferase, mitochondrial	*GOT2*	4.42	.0044962
Proteasome subunit α type-6	*PSMA6*	4.39	.0317503
Heat shock protein HSP 90-α	*HSP90AA1*	4.33	.0000011
Coronin-1C	*CORO1C*	4.26	.0000013
Eukaryotic initiation factor 4A-I	*EIF4A1*	4.24	.0059134
Transgelin-2	*TAGLN2*	4.20	.0022821
Heat shock cognate 71-kilodalton protein	*HSPA8*	4.20	.0125521
Nucleoside diphosphate kinase B	*NME2*	4.15	.0049568
Actin, cytoplasmic 2	*ACTG1*	4.08	.0000034
Neuropilin-2	*NRP2*	4.06	.0175685
Pentraxin-related protein PTX3	*PTX3*	4.04	.0007182
Nucleolin	*NCL*	4.01	.0276738
Filamin-A	*FLNA*	4.01	.0003733

Table 1. Continued

Protein names	Gene names	Moy ratio NT/SOM230	P value
Fibromodulin	FMOD	3.98	.0092232
Plasminogen activator inhibitor 1	SERPINE1	3.97	.0000854
Chloride intracellular channel protein 4	CLIC4	3.92	.0008258
Multiple inositol polyphosphate phosphatase 1	MINPP1	3.91	.0418345
Neuropilin-1	NRP1	3.91	.0167928
Heat shock protein HSP 90-β	HSP90AB1	3.91	.0000448
14-3-3 protein Σ	SFN	3.88	.0010093
Heterogeneous nuclear ribonucleoprotein D0	HNRNPD	3.84	.0028596
Reticulocalbin-1	RCN1	3.83	.0001862
Vimentin	VIM	3.81	.0081098
Putative elongation factor 1-α-like 3	EEF1A1P5	3.80	.0005683
Lumican	LUM	3.80	.0000514
Exostosin-2	EXT2	3.79	.0233352
Puromycin-sensitive aminopeptidase	NPEPPS	3.79	.0045265
Glutaminyl-peptide cyclotransferase	QPCT	3.76	.0074783
Pyruvate kinase PKM	PKM	3.76	.0006099
C-Jun-amino-terminal kinase-interacting protein 4	SPAG9	3.74	.0003581
Poly(rC)-binding protein 1	PCBP1	3.71	.0004751
Farnesyl pyrophosphate synthase	FDPS	3.55	.0033517
Tropomyosin α-4 chain	TPM4	3.53	.0022587
Transitional endoplasmic reticulum adenosine triphosphatase	VCP	3.52	.0000575
Hyaluronan-binding protein 2	HABP2	3.50	.0021050
Serglycin	SRGN	3.49	.0041091
Metalloproteinase inhibitor 2	TIMP2	3.46	.0000760
Phosphoglucomutase-1	PGM1	3.43	.0083578
Filamin-C	FLNC	3.42	.0073859
Heat shock 70-kilodalton protein 6	HSPA6	3.42	.0002413
78-kilodalton glucose-regulated protein	HSPA5	3.36	.0206891
Dihydropyrimidinase-related protein 2	DPYSL2	3.36	.0000008
Protein CYR61	CYR61	3.33	.0021073
Chloride intracellular channel protein 1	CLIC1	3.32	.0000008
α-actinin-1	ACTN1	3.29	.0025329
Histone H2A type 2-C; histone H2A type 2-A	HIST2H2AC	3.29	.0061036
Ubiquitin carboxyl-terminal hydrolase isozyme L1	UCHL1	3.28	.0423517
Proteasome subunit α type-1	PSMA1	3.20	.0008972
Ras-related protein Rap-1A	RAP1A	3.19	.0000007
Gremlin-1	GREM1	3.18	.0497429
γ-glutamyl hydrolase	GGH	3.17	.0003584
14-3-3 protein η	YWHAH	3.17	.0004627
Peroxiredoxin-1	PRDX1	3.14	.0000143
Protein SET	SET	3.14	.0011534
Protein CutA	CUTA	3.09	.0021038
Peptidyl-prolyl cis-trans isomerase A	PPIA	3.09	.0071350
Galectin-1	LGALS1	3.08	.0000155
Protein disulfide-isomerase	P4HB	3.08	.0009140
F-actin-capping protein subunit α-1	CAPZA1	3.05	.0000032
Histone H2B type 1-L	HIST1H2BL	3.01	.0104479
Thrombospondin-3	THBS3	3.01	.0061737
α-actinin-4	ACTN4	2.99	.0006276
Procollagen-lysine, 2-oxoglutarate 5-dioxygenase 1	PLOD1	2.99	.0000104

Table 1. Continued

Protein names	Gene names	Moy ratio NT/SOM230	*P* value
Acylamino-acid–releasing enzyme	APEH	2.97	.0382093
Lysyl oxidase homolog 2	LOXL2	2.96	.0002226
Thrombospondin-4	THBS4	2.92	.0017107
Procollagen-lysine, 2-oxoglutarate 5-dioxygenase 2	PLOD2	2.90	.0165680
Glyceraldehyde-3-phosphate dehydrogenase	GAPDH	2.89	.0000848
Calmodulin	CALM1	2.89	.0223212
X-ray repair cross-complementing protein 5	XRCC5	2.88	.0123259
Phosphoglycerate kinase 1	PGK1	2.81	.0111379
14-3-3 protein γ	YWHAG	2.77	.0000012
Collagen α-1(VI) chain	COL6A1	2.72	.0001905
Rho guanine nucleotide exchange factor 18	ARHGEF18	2.66	.0000016
Malate dehydrogenase, cytoplasmic	MDH1	2.66	.0185247
Triosephosphate isomerase	TPI1	2.63	.0036592
Fructose-bisphosphate aldolase A	ALDOA	2.59	.0288449
Vinculin	VCL	2.54	.0021035
α-enolase	ENO1	2.51	.0004602
Apolipoprotein C-III	APOC3	2.46	.0180784
Secernin-1	SCRN1	2.45	.0288882
Ubiquitin-60S ribosomal protein L40	UBA52	2.39	.0001326
14-3-3 protein β/α	YWHAB	2.38	.0002045
DnaJ homolog subfamily C member 13	DNAJC13	2.38	.0120707
14-3-3 protein epsilon	YWHAE	2.37	.0002483
Moesin	MSN	2.35	.0003671
Phosphoglycerate mutase 1	PGAM1	2.24	.0024083
Nicotinamide N-methyltransferase	NNMT	2.22	.0153174
Ferritin heavy chain	FTH1	2.20	.0224213
Aldose 1-epimerase	GALM	2.18	.0006598
Nuclear receptor subfamily 1 group D member 2	NR1D2	2.02	.0248565

NOTE. n = 9 CAF primary cultures, *P* < .05.
IQGAP1, IQ Motif Containing GTPase Activating Protein 1; NSF, N-Ethylmaleimide-Sensitive Factor.

significantly triggers DNA damage (phospho-γ-H2AX index, H2A histone family member X), and did not affect tumor cell proliferation (Ki-67 index) (Figure 6A–C). When exploring drug effects on the stroma, we observed that the combination therapy did not affect the presence of intratumor CD8-positive lymphocytes, or myeloid lymphocyte antigen 6 complex locus G–positive and myeloperoxidase-positive granulocytes, as compared with gemcitabine (Figure 6D–F), but significantly decreased CD206-positive myeloid cell number, a read-out of TAMs (Figure 6G and H). αSMA-positive CAFs and ECM (glycosaminoglycan and collagen) deposits (quantified in turquoise blue/green using the Movat Pentachrome stain) were robustly decreased with the combination therapy, as compared with gemcitabine (Figure 6I–L). Tumor cell STAT3 (signal transducer and activator of transcription member 3) phosphorylation, a reported marker of ECM-induced mechanical stress and of increased tumor cell invasiveness,[25] followed the same pattern as ECM deposits (Figure 6M). Gemcitabine tends to increase vessel area (using a monoclonal mouse-specific panendothelial cell antigen antibody [MECA32]), and to decrease pericyte recruitment around tumor vessels (as quantified using the co-stain of MECA32 and neuron-glial antigen 2 [NG2]), effects that are significantly reversed when SOM230 is combined (Figure 6N–P). Interestingly, pericyte depletion was reported to induce metastasis.[26] In liver metastases, CD206-positive myeloid cell number also was decreased by the combination therapy as compared with gemcitabine (Figure 7A and B), as well as αSMA-positive cells (Figure 7C and D), whose number increased with metastasis size (Figure 7E). Altogether, our results show in KPC mice that SOM230 normalizes the immune monocytic, fibrotic, and vascular stroma, in correlation with its anti-metastatic potential.

When searching for factors commonly down-regulated by SOM230 in the CAF secretome (Table 1), in the plasma of drug-treated grafted mice (Table 2), and in the plasma of KPC mice also treated with gemcitabine (Figure 7F–H,
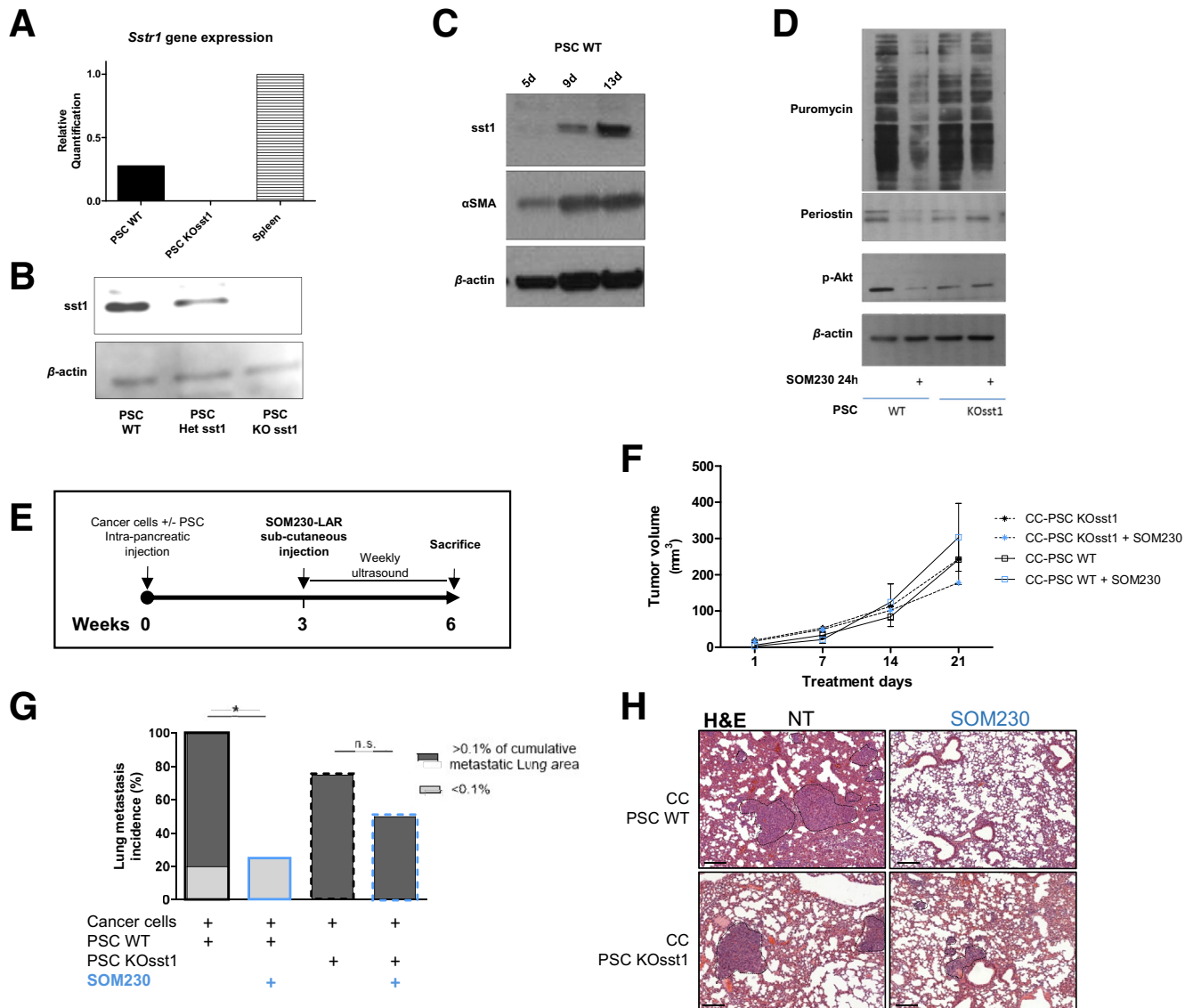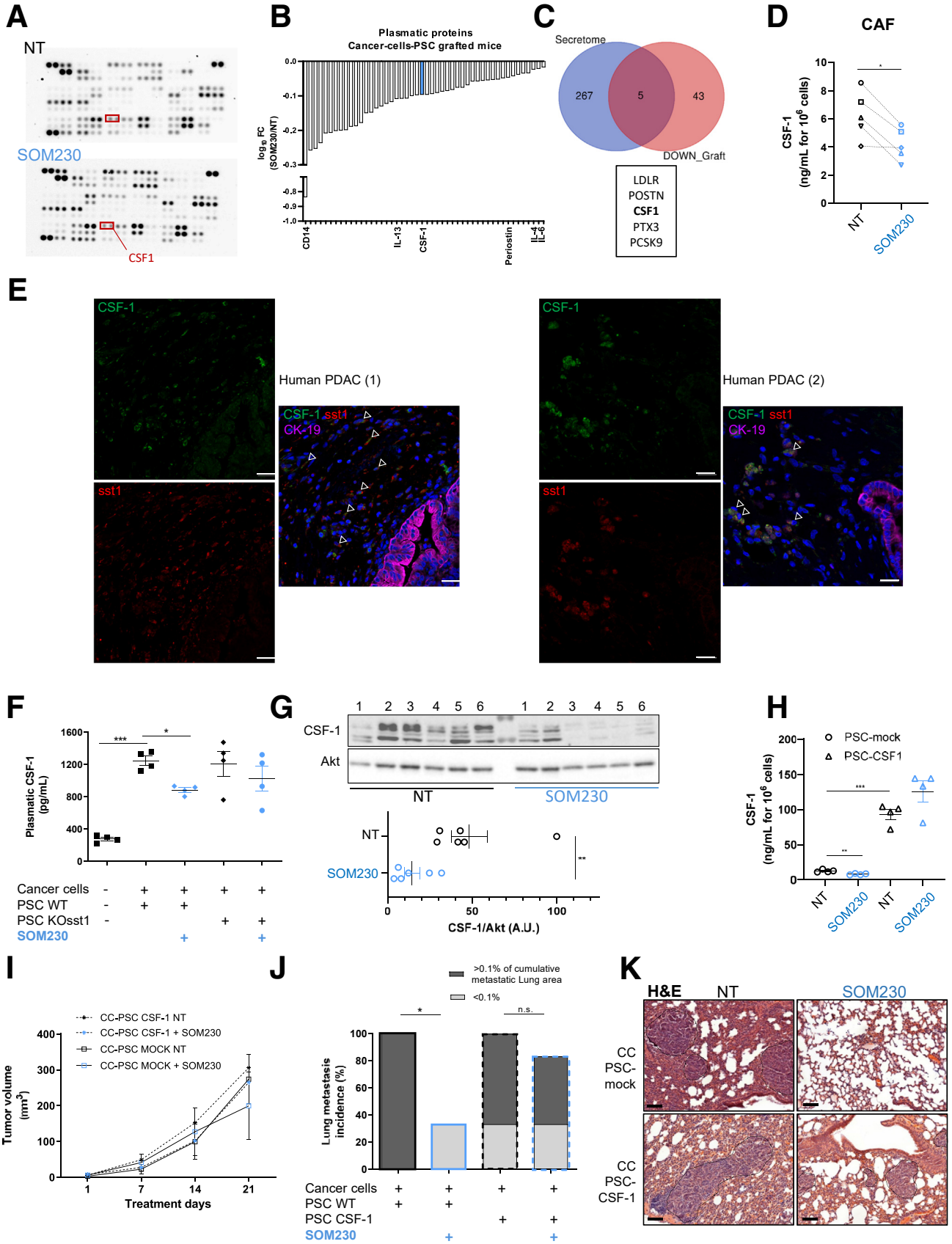
Figure 2. SOM230 reduces metastasis dependently on CAF-expressed sst1 in a murine PDA model. (*A–D*) Characterization of WT and KOsst1 murine PSCs. (*A*) The abundance of sstr1 mRNA was analyzed by real-time quantitative PCR in WT or KOsst1 PSCs, and in spleen as a positive control, and normalized to the housekeeping rps16 mRNA. (*B*) Western blot analyses of the indicated proteins in PSCs, either WT, heterozygous (Het sst1), or KO sst1. β-actin was used as an internal loading control. (*C*) Western blot analyses of the indicated proteins in PSCs freshly isolated from mouse pancreata and cultured for 5, 9, and 13 days. (*D*) Western blot analyses of the indicated proteins in WT or KOsst1 PSCs, treated or not with SOM230 (10^{-7} mol/L; 24 h). β-actin was used as an internal loading control. (*E*) Experimental design of the study. Cancer cells (CC) were syngeneically and orthotopically co-grafted with murine sst1-WT or sst1-KO PSCs (PSC KOsst1). After 3 weeks, mice were randomized and treated or not (NT) with SOM230–long-acting releasing form (LAR) for 3 weeks. After 6 weeks, mice were killed (n = 4–6 mice/group). (*F*) Tumor volume evolution from treatment day 1 to day 21, monitored weekly by ultrasound, in mice grafted with CCs plus WT or KOsst1 PSCs. (*G*) Metastasis incidence in mouse lungs and distribution of mice according to their metastatic lung load (cumulative metastatic lung area less than or greater than 0.1% of total lung area). The chi-squared test was used to generate *P* values. *$P < .05$. (*H*) Representative H&E staining of mouse lungs. *Dashed lines* encircle metastases. *Scale bars*: 100 μm.

Table 4), we again retrieved CSF-1 among 5 other proteins, also including periostin (Figure 7H). Hence, in KPC mice, SOM230 reduced plasma or intratumor CSF-1 expression when combined with gemcitabine compared with gemcitabine alone (Figure 7I and J). Interestingly, CSF-1 plasmatic concentration in KPC mice correlated with the extent of liver metastatic load (Figure 7K). In KPC primary tumors, αSMA-

positive CAFs, but barely tumor cells, expressed CSF-1 (Figure 7L). However, in KPC liver metastases, CSF-1 was expressed heterogeneously, mainly in stromal cells (cytokeratin-19–negative but also αSMA-negative) in large metastases (>0.7 mm^2) (Figure 7M, 3 upper panels), but mainly in tumor cells (cytokeratin-19–positive), with a membranous localization, in smaller metastases (<0.7 mm^2)

A NT / SOM230

B Plasmatic proteins
Cancer-cells-PSC grafted mice

C Secretome / DOWN_Graft
267 5 43

LDLR
POSTN
CSF1
PTX3
PCSK9

D CAF

E CSF-1 / sst1 / CSF-1 sst1 CK-19 — Human PDAC (1)

CSF-1 / sst1 / CSF-1 sst1 CK-19 — Human PDAC (2)

F Plasmatic CSF-1 (pg/mL)

Cancer cells
PSC WT
PSC KOsst1
SOM230

G CSF-1 / Akt — NT / SOM230

CSF-1/Akt (A.U.)

H PSC-mock / PSC-CSF1

I Tumor volume (mm³) — Treatment days

CC-PSC CSF-1 NT
CC-PSC CSF-1 + SOM230
CC-PSC MOCK NT
CC-PSC MOCK + SOM230

J Lung metastasis incidence (%)

>0.1% of cumulative metastatic Lung area
<0.1%

Cancer cells
PSC WT
PSC CSF1
SOM230

K H&E NT / SOM230

CC PSC-mock

CC PSC-CSF-1

(Figure 7M, 3 lower panels). Altogether, in a spontaneous PDA murine model, these results confirmed that SOM230 provides a therapeutic antimetastatic benefit when given in combination with gemcitabine, in correlation with a drug inhibitory effect on the chemokine CSF-1. Our results also show that the CSF-1 plasmatic concentration correlates with the metastatic potential in KPC mice, and that CSF-1 is expressed mainly in the stroma in KPC primary tumors and large stroma-rich metastases.

CSF-1 Is a Stromal Marker of Patient PDA Aggressiveness and Metastasis

To link *CSF-1* expression with clinical parameters and biological tumor phenotypes in PDA patients, and because *CSF-1* mRNA may be expressed by both human tumor cells and stromal CAFs, we investigated 2 public RNA sequencing (RNAseq) databases, in which epithelial and stromal genes are quantified separately[5,27]: first, the Maurer et al[27] database, in which RNAseq were run on patient PDA microdissected-stromal and epithelial lesions (n = 65 patients) (Figure 8A–G); and, second, the patient-derived xenograft RNAseq (PaCaOmics patient-derived xenografts [PDX], n = 30), in which human and mouse gene sequences, originating from the tumor's epithelial or stromal compartment, respectively, are distinguishable[5] (Figure 8H–L). In both databases, we found *CSF-1* mRNA to be significantly more abundant in the stromal than in the epithelial compartment (Figure 8A and H). Moreover, high levels of stromal *CSF-1* mRNA correlated significantly with high American Joint Committee on Cancer tumor staging (patient cohort) (Table 5), or with clinical parameters of disease progression, that is, nonresectability status (PDX cohort) (Figure 8I), which is not the case for epithelial *CSF-1* mRNA (Table 5, Figure 8J). Molecularly, high stromal *CSF-1* mRNA expression correlated positively with signatures of aggressive "stroma-activated" (Figure 8B) and "epithelial basal-like" tumors (Figure 8C and K), and negatively with more-differentiated "epithelial classical-like" signatures (Figure 8D).[4-6] High epithelial *CSF-1* mRNA expression also was associated significantly with stroma-activated signatures (Figure 8E), but not consistently with signatures of the tumoral epithelium (basal, classic) because the link was observed in PDX (Figure 8L), but not in microdissected, lesions (Figure 8F and G). Such correlative analyses then were validated using a third patient cohort (PDA resected tissues from n = 38 patients) in which a CSF-1 protein immunohistochemistry score was quantified in both the tumor epithelial and stromal compartments (Figure 8M–Y). CSF-1 protein was expressed in both the epithelial and stromal compartments, the latter also was αSMA positive (Figure 8M). Clinically, patients with a high metastatic lymph node ratio (LNR) presented with significantly higher stromal, but not epithelial, CSF-1 scores (Figure 8N). Accordingly, patients with high stromal CSF-1 scores tended to have a shorter life expectancy (P = .11) (Figure 8X), which was not the case for high epithelial CSF-1 patients (Figure 8Y). Pathologically, tumors classified with a high activated stroma index[28] or CD163 (TAM marker) scores also presented with significantly increased stromal, but not epithelial, CSF-1 scores (Figure 8O and P). Conversely, CD8 scores were not linked to either stromal or epithelial CSF-1 scores (Figure 8Q). Molecularly, high stromal or epithelial CSF-1 scores correlated positively with stromal RNAseq signatures of activated stroma or of activated/inflamed stroma, respectively (Figure 8R and S), whereas high stromal CSF-1 scores only correlated negatively with RNAseq signatures of inactivated/structured stroma (Figure 8T) and of epithelial classic-like tumors (Figure 8V). No correlation was found between stromal or epithelial CSF-1 scores with RNAseq signatures of immune stroma (Figure 8U) or of epithelial basal-like tumor (Figure 8W). Altogether, these results show that a high stromal CSF-1 score correlated consistently with stromal activities recognized as being of

---

Figure 3. (*See previous page*). **SOM230 reduces tumoral and plasmatic CSF-1 expression dependently on CAF-expressed sst1, explaining its antimetastatic effect in murine PDA models.** (*A*) Membrane antibody arrays using plasma from mice grafted with cancer cells (CCs) plus PSCs, and treated or not (NT) with SOM230 (pool of n = 5 mice/membrane). (*B*) Cytokine array quantification of plasma proteins in CCs plus PSC grafted mice and treated with SOM230 as compared with untreated (NT), showing down-regulated proteins (pool of n = 5 mice/group). (*C*) Venn diagram of the overlap of down-regulated plasma proteins from grafted mice identified in cytokine arrays (*A, B*) and from CAF secretome analysis (Table 1). Common proteins are listed underneath. (*D* and *H*) CSF-1 ELISA quantification in (*D*) conditioned media of human CAF (n = 5 CAF primary cultures), or (*H*) murine PSC overexpressing CSF-1 or not (mock) (performed in quadruplicate), treated or not (NT) with SOM230, and expressed relative to NT. The paired or unpaired Student t test was used. (*E*) Immunofluorescence confocal analysis of CSF-1 (green), sst1 (red), and cytokeratin-19 (CK-19; purple) expression in 2 patient-derived PDA tissues, showing co-localization in the stroma (at distance from tumor epithelial CK-19–positive cells) of sst1 and CSF-1. *Scale bars:* 50 μm. (*F*) Plasma CSF-1 ELISA quantification at death of ungrafted mice (first condition), or grafted mice treated or not with SOM230 (from Figure 2, n = 4 per group). Each *dot* represents the CSF-1 plasma concentration measured in 1 mouse. Analysis of variance followed by the Bonferroni multiple comparison post-test was used to generate P values. (*G*) Western blot analysis of tumor lysates from grafted mice (from Figure 2, mouse tumors 1-to-6) treated or not (NT) with SOM230 (n = 6 mice/treatment condition), with anti–CSF-1 or Akt (loading control) antibody, and quantification (densitometric analysis) of CSF-1 normalized to Akt expression (A.U., arbitrary unit). The unpaired Student t test was used to generate P values. (*I–K*) CCs were syngeneically and orthotopically co-grafted with murine PSCs overexpressing or not (MOCK) a secreted CSF-1 form (PSC–CSF-1). After 3 weeks, mice were randomized and treated or not (NT) with SOM230-LAR for 3 weeks. After 6 weeks, mice were killed (n = 6 mice/group). (*I*) Tumor volume evolution from treatment day 1 to 21, monitored weekly by ultrasound. (*J*) Metastasis incidence in mouse lungs and distribution of mice according to their metastatic lung load (cumulative metastatic lung area less than or greater than 0.1% of the total lung area). The chi-squared test was used to generate P values. (*K*) Representative H&E staining of mouse lungs. *Dashed lines* encircle metastases. *Scale bars*: 100 μm. *P < .05, **P < .01, and ***P < .001

poor prognosis for PDA patients,[4,6] alongside increased tumor cell aggressiveness (less-differentiated phenotype), which, however, was not the case for the epithelial CSF-1 score.

Table 2. Listing of Down-Regulated Proteins in Cancer Cell–PSC Grafted Mice Plasma: SOM230 vs Untreated

Protein name	Log ratio SOM230/NT
CD14	-0.836393
IFN-γ	-0.257125
TIM-1	-0.2522933
IL5	-0.2357543
Chemerin	-0.2076414
PDGF-BB	-0.2058304
IL10	-0.2005681
Leptin	-0.1993592
Serpin F1	-0.1981243
Flt-3 ligand	-0.1887131
CD160	-0.1865666
CXCL9	-0.1772411
TNF-α	-0.1492109
Myeloperoxidase	-0.1471288
Pentraxin 2	-0.1347746
E-selectin	-0.1293948
IL12p40	-0.121981
FGF acidic	-0.1169429
IL13	-0.1077902
LDL R	-0.1072964
VCAM-1	-0.1065818
IL11	-0.09950715
PD-ECGF	-0.09708886
M-CSF	-0.09599823
RBP4	-0.095954
LIF	-0.09346522
PCSK9	-0.09068561
CCL11	-0.08666945
IL1 α	-0.08475557
IGFBP-3	-0.08151417
IL27p28	-0.0749929
CXCL11	-0.07498571
RAGE	-0.06808221
CXCL10	-0.05732954
Pentraxin 3	-0.05685075
Endoglin	-0.05549461
IL7	-0.05403424
Pref-1/DLK-1	-0.0525299
P-selectin	-0.05165642
IGFBP-5	-0.04817382
IL15	-0.04627419
Periostin	-0.04173948
Lipocalin-2	-0.03777582

Table 2. Continued

Protein name	Log ratio SOM230/NT
IL28	-0.03427079
Osteopontin	-0.033357
IL33	-0.02293778
IL4	-0.02049208
IL6	-0.01649792

NOTE. Pool of n = 5 mice/group.
CCL, CC chemokine ligand; CXCL, (C-X-C) motif ligand; DLK-1, delta-like protein 1; FGF, fibroblast growth factor; Flt-3, fms like tyrosine kinase 3; IFN, interferon; IGFBP, insulin-like growth factor- binding protein; IL, interleukin; LDL, low-density lipoprotein; LIF, leukemia inhibitory factor; PCSK9, proprotein convertase subtilisin/kexin type-9; PD-ECGF, platelet-derived endothelial cell growth factor; PDGF-BB, platelet-derived growth factor-BB; RAGE, receptor for advanced glycation end products; RBP-4, retinol-binding protein 4; TIM-1, T cell Ig and mucin 1; TNF, tumor necrosis factor; VCAM-1, vascular cell adhesion molecule 1.

Discussion

CAFs are master players in the secretion of proteins regulating the tumor microenvironment. Through secretome MS analyses on media conditioned by 9 primary CAF cultures, here we identified CAF-secreted proteins, which are under the negative control of SOM230. Among them, 47 were found commonly in stroma-activated signatures published for human PDA.[4,6] Such concurrent inhibition by SOM230 of several CAF protumoral signals was consistent with the robust antimetastatic effect that we obtained in 2 different immunocompetent mouse PDA models, and most certainly provided a therapeutic advantage in comparison with specific pharmacologic inhibitors or blocking antibodies, which are directed against 1 specific factor or receptor. This is particularly essential in PDA, in which many single-target drug therapies thus far have failed, even when combined with chemotherapies (eg, hedgehog pathway inhibitor,[29] or pegvorhyaluronidase alfa [PEGPH20][30]). A combination of several drugs seems necessary to reach efficacy in PDA, at the cost of safety and adverse effects for patients. SOM230 represents a safe drug (Food and Drug Administration–approved for neuroendocrine Cushing tumors and safely tested in a phase-I PDA trial in combination with gemcitabine[31]), with a pharmacologic inhibitory action on sst1-expressing CAFs, abrogating CAF cross-talk with tumor and other stromal cells.

Why SOM230 alone is not as effective at inhibiting metastasis in KPC mice as when it is combined with gemcitabine is intriguing. Gemcitabine was reported to alter the pancreatic immune, fibrotic, and vascular stroma,[19,32,33] de novo triggering a metastatic microenvironment.[34,35] SOM230 did not improve gemcitabine-induced cytotoxicity in tumor cells, but normalized the gemcitabine-remodeled stroma, reducing stellate cell activity, tumor-associated macrophage presence, ECM deposits, and angiogenesis.
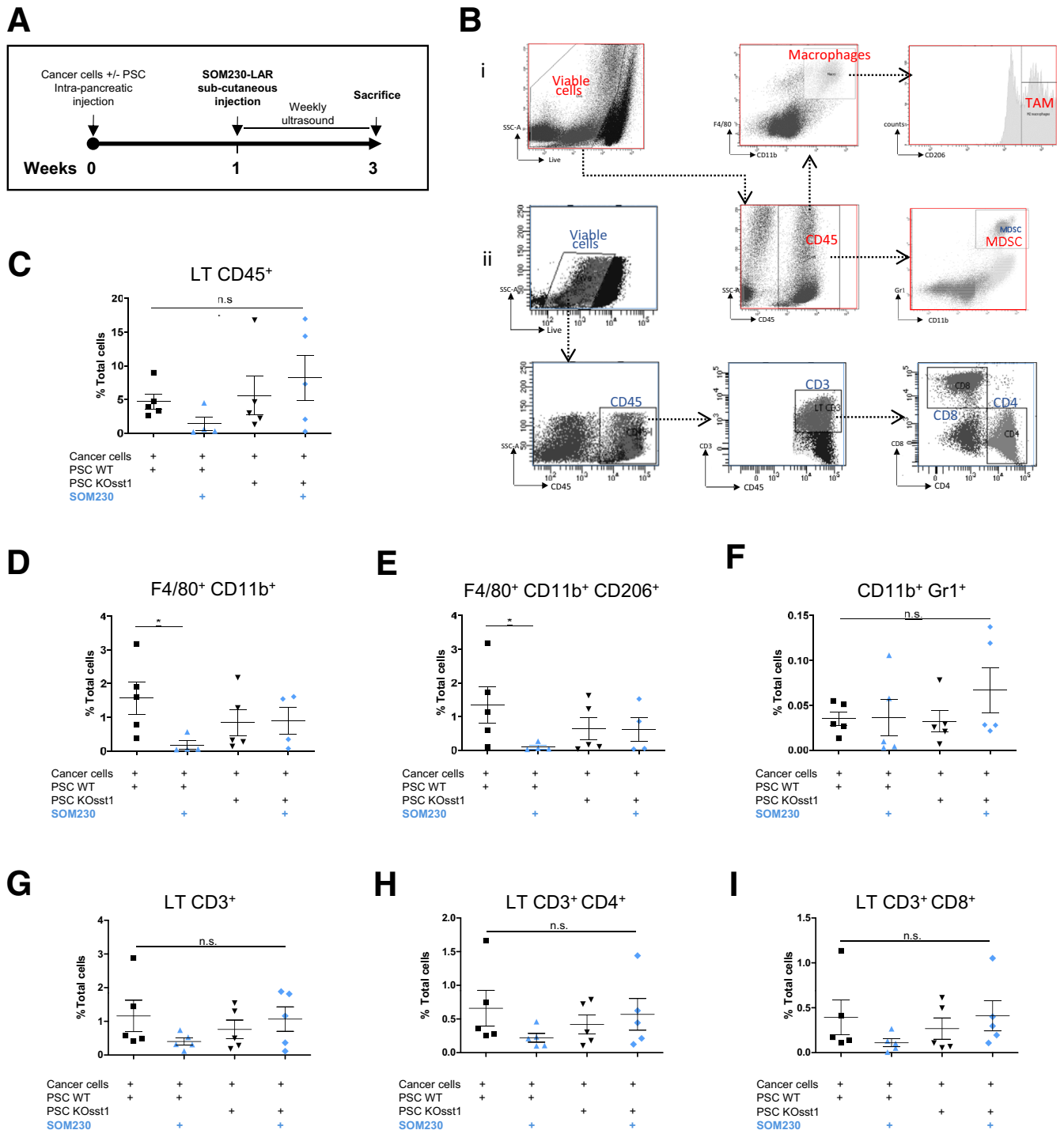
Figure 4. SOM230 reduces TAM presence. (A and B) Experimental design of the study. (A) Cancer cells were syngeneically and orthotopically co-grafted with murine WT or KOsst1 PSCs. One week after graft, mice were randomized and treated or not with SOM230-LAR. Three weeks after graft, mice were killed. (B) Gating strategy to identify viable cells, total CD45-positive cells, total macrophages, CD206high macrophages, and myeloid-derived suppressor cell immune populations (i, red boxes), or total CD45-positive cells, total lymphocytes, helper CD4 lymphocytes, and cytotoxic CD8 lymphocytes immune populations (ii, blue boxes). (C–I) Proportions of (C) total immune cells (CD45+ cells), (D) total macrophages (CD45+; F4/80+; CD11b+ cells), (E) CD206hi macrophages, (F) myeloid-derived suppressor cell (CD45+; CD11b; lymphocyte antigen 6 complex locus G [Ly6g]+ cells), (G) T lymphocytes (CD45+; CD3+ cells), (H) helper T lymphocytes (CD4+ T lymphocytes), and (I) cytotoxic T lymphocytes (CD8+ T lymphocytes) were quantified (in % of total cells) by flow cytometry on tumors from cancer cells + PSC-injected mice (n = 4–5 mice/group). The Kruskal–Wallis test followed by the Dunn multiple comparison post-test was used to generate P values. *P < .05.
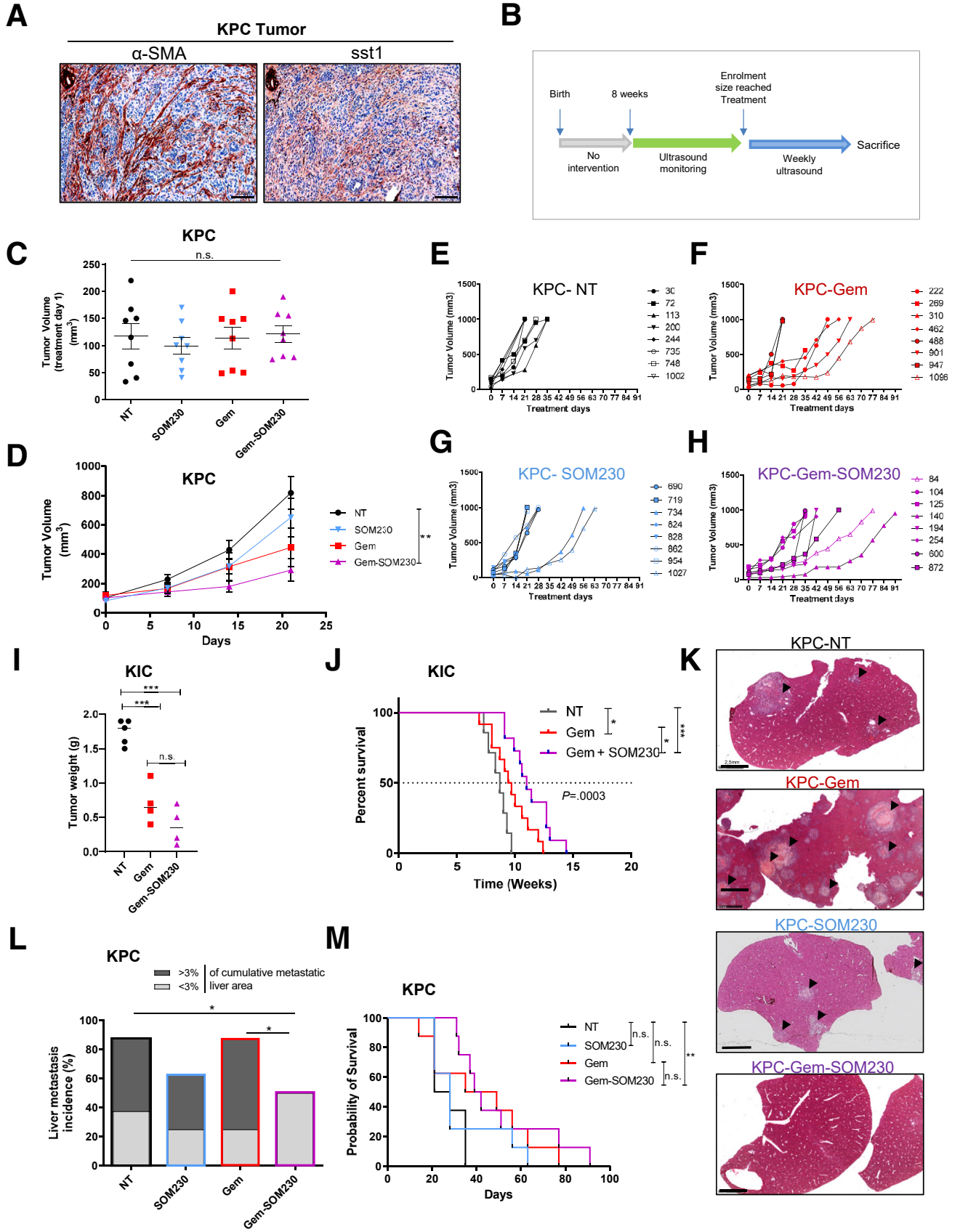
Table 3. Characteristics of KPC Mice

Drug	ID	Age at treatment start, d	Tumor volume on treatment day 1, mm^3	Tumor volume at death, mm^3	Survival, d	Liver metastasis	Liver metastatic area, %	Ascites
No	30	203	150	~1000	21	Yes	0.02	Yes
	72	203	146	~1000	35	Yes	0.24	No
	113	161	34	~1000	42	No	0.00	No
	200	133	66	~1000	35	Yes	0.11	No
	748	131	167	~1000	30	Yes	4.72	Yes
	735	175	40	~1000	21	Yes	6.94	Yes
	244	210	113	~1000	20	Yes	36.40	Yes
	1002	114	115	~1000	23	Yes	4.98	Yes
SOM230	828	205	145	~1000	21	Yes	0.06	No
	862	210	101	~1000	16	No	0.00	No
	1027	164	53	~1000	56	No	0.00	No
	824	247	41	~1000	52	Yes	2.92	No
	954	238	170	~1000	22	Yes	5.79	Yes
	719	143	113	~1000	21	Yes	10.74	Yes
	734	156	99	~1000	21	No	0.00	No
	690	126	72	~1000	24	Yes	7.35	No
Gemcitabine	310	162	200	~1000	20	Yes	28.15	No
	222	162	31	~1000	37	Yes	0.04	No
	269	172	149	560	50	Yes	59.03	No
	462	205	195	~1000	46	Yes	11.89	Yes
	488	273	108	~1000	13	Yes	9.75	Yes
	947	204	144	~1000	21	No	0	Yes
	901	233	50	700	60	Yes	1.44	No
	1096	148	53	~1000	80	Yes	5.99	No
Gemcitabine SOM230	104	210	158	~1000	31	No	0.00	No
	254	145	123	~1000	39	Yes	0.05	No
	125	267	190	~1000	32	Yes	0.46	No
	140	192	32	800	91	No	0.00	No
	194	212	80	~1000	42	Yes	2.86	Yes
	953	194	90	~1000	77	No	0.00	No
	600	197	111	~1000	37	Yes	0.35	Yes
	872	150	78	~1000	51	No	0.00	Yes

We focused on the CSF-1 chemokine, which was down-regulated by SOM230 in CAF secretomes and in PDA harboring mouse plasma. CSF-1 is involved in intratumor recruitment of monocytes, and in their polarization into macrophages, endowed with pro-angiogenic and ECM remodeling features that favor tumor cell metastasis.[24,36] In PDA patients, high serum CSF-1 levels were correlated with advanced tumor stages.[37] Accordingly, we observed that the plasma CSF-1 level correlated with liver metastatic load in KPC mice. SOM230 treatment decreased intratumor and plasma CSF-1 levels, consistent with fewer intratumor macrophages. In vitro, CAFs were reported to cross-talk

Figure 5. (*See previous page*). **SOM230 delays the growth and metastasis of spontaneous pancreatic tumors generated in the immunocompetent KPC mouse model.** (*A*) Representative immunostaining of αSMA and sst1 receptor in serial sections of a KPC primary tumor (untreated mice) showing expression of sst1 receptor in αSMA-positive cell areas. *Scale bars*: 200 μm. (*B–H*) Experimental design. (*B*) KPC mice had an ultrasound weekly from 8 weeks of age until tumor size enrollment was reached (homogenous treatment group tumor volumes, 31–200 mm³; mean, 103.9 mm³; analysis of variance followed by the Bonferroni multiple comparison post-test was used). (*C*) Mice were randomized into treatment groups (PBS-treated [NT], SOM230-long-acting release [LAR], gemcitabine [Gem], or gemcitabine plus SOM230-LAR [Gem-SOM230], n = 8 mice per group). (*D–H*) Tumor volume was quantified by ultrasound until ethical end point (when maximal-authorized volume of the primary tumor, or clinical end points, were reached). Tumor volume progression from treatment day 1 to 21. Analysis of variance followed by the Bonferroni multiple comparison post-test was used to generate *P* values. (*D*) Representation of tumor volume progression from treatment day 1 until death for each mouse in the 4 treatment conditions. (*E–H*) KPC mouse identity numbers are indicated, according to Table 3. (*I* and *J*) Pdx1-Cre; LSL-KrasG12D; Ink4a$^{fl/fl}$ mice (KIC) were treated as indicated. (*I*) Tumor weight was measured at euthanasia (n = 4–5 mice/group) (analysis of variance followed by the Bonferroni multiple comparison post-test was used to generate *P* values). (*J*) Survival analysis (Kaplan–Meier) was analyzed using a log-rank test. (*K–M*) KPC liver metastasis and mouse survival analyses. (*K*) Representative H&E staining. *Arrows* indicate metastases. *Scale bars*: 2.5 mm. Metastasis incidence in KPC livers and distribution of mice according to their metastatic liver load (cumulative metastatic liver area less than or greater than 3% of the total liver area). (*L*) Significance of liver metastatic overload (>3% of the total liver area) was determined with the chi-squared test. (*M*) Survival analysis of KPC mice treated as indicated. Kaplan–Meier survival data were analyzed using a log-rank test. *$P < .05$, **$P < .01$, and ***$P < .001$.
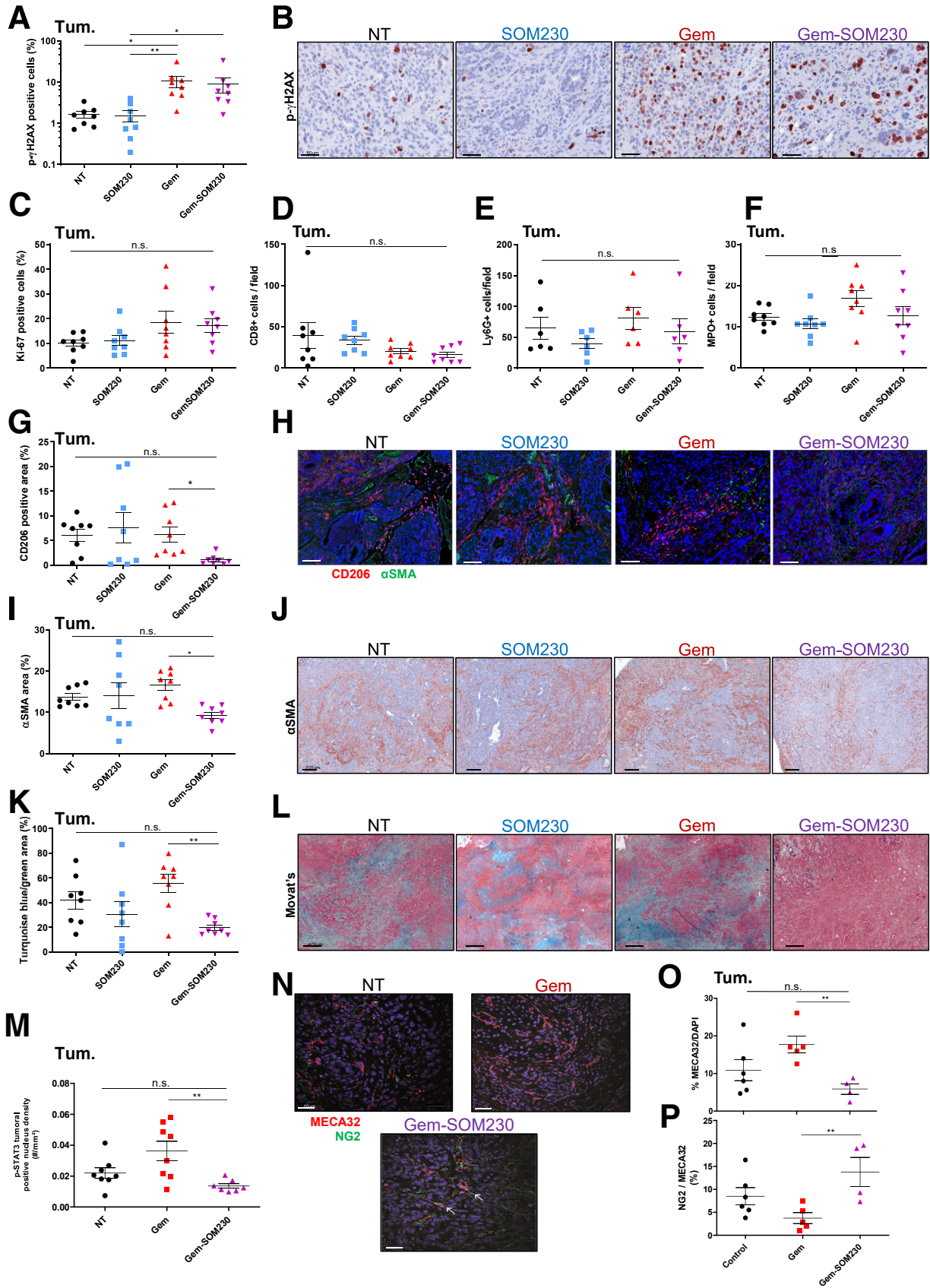
with macrophages pushing toward the M2 phenotype through CAF-derived CSF-1.[12,38] We showed that the SOM230 antimetastatic effect relied on CAF-expressed sst1, and on the drug inhibitory effect of CAF-secreted CSF-1.

In preclinical studies, CSF-1 receptor (CSF-1-R) blockade using CSF-1-R inhibitors or blocking antibodies resulted in a shift from mostly immunosuppressive to improved antigen presentation capacities of tumor-associated macrophage subsets, with a therapeutic benefit for different solid tumors including PDA, when associated with chemotherapy or radiotherapy.[36] In PDA, the CSF-1-R blockade decreased tumor growth through increased intratumor cytotoxic CD8 T-cell recruitment,[39] and synergized with checkpoint-based immunotherapies.[40] SOM230 alone or in combination with gemcitabine did not increase intratumor CD8 T-cell recruitment in 2 PDA mouse models, even though it decreased plasma and intratumor CSF-1, and was antimetastatic. CSF-1-R blockade recently was shown to trigger transcriptomic reprogramming of PDA tumor cells to a more differentiated and less-aggressive PDA subtype,[11] stressing the critical role of CSF-1-R–expressing macrophages in driving PDA tumor cell plasticity, in addition to their role in blocking T-cell responses. This is consistent with our observation that CSF-1 mRNA or protein expression, when quantified specifically in the stroma, correlates with markers of aggressiveness, that is, clinical markers (tumor stage, LNR), pathologic markers (activated stroma index, CD163-positive macrophage presence), and molecular markers (activated status of the stroma, increased basal-like and/or decreased classic-like tumor cell phenotype). However, we could not correlate epithelial CSF-1 mRNA or protein expression with an inactivated status of the stroma as it was recently reported in pure (stroma-poor) basal-like tumors.[41] A possible explanation is that our immunohistochemistry PDA cohort did not include rare pure basal-like tumors. Indeed, it comprised 29% of basal-like tumors and 71% of classic-like tumors, which harbor either an activated stroma (19% and 17%, respectively) or a desmoplastic stroma (10% and 32%, respectively), or poor stroma content for 22% of pure classic tumors, as previously described.[6] We observed that epithelial CSF-1 expression correlated with the presence of CD163-positive macrophages and with a molecular "activated/inflamed" stroma status recognized to be of bad prognosis in classic tumors.[6] PDA stroma seemed to be the principal source of CSF-1, at least when quantified at the mRNA level in 2

independent PDA cohorts, which was consistent with a recently described CSF-1–expressing immunomodulatory CAF subset identified in melanomas.[42] CSF-1 protein quantification (by immunohistochemistry) from a third PDA cohort indicated a higher epithelial rather than stromal source, although this may have been biased by differences in antibody recognition of the membranous (uncleaved) and soluble (cleaved) CSF-1 forms, which could be distributed differently in the epithelial and stromal compartments (eg, we observed a membranous expression of CSF-1 in KPC liver metastatic tumor cells) (Figure 7M). How and where the membranous CSF-1 protein is cleaved, releasing the soluble chemoattractant factor, and whether membranous and soluble CSF-1 have similar functions in tumors, are as yet unresolved but important issues to understand.

Altogether, our results show that antimetastatic SOM230 pharmacotherapy should benefit PDA patients enrolled in chemotherapeutic protocols, the effect of SOM230 could be explained mechanistically by a broad inhibitory action on CAF cross-talk with tumor and nontumor cells, including macrophages through CSF-1.

Methods

Cell Lines and Primary CAF Cultures

KPC cells were derived from PDA tumor tissue obtained from LSL-KrasG12D/+; LSL-Trp53R172H/+; p48-Cre+/- mice (C57BL/6 background, a generous gift from Professor D. Saur, Technische University of Munich). PSCs were isolated from mouse pancreata, either WT or KOsst1 (a generous gift from Dr C. Viollet, INSERM U1266, Institute of Psychiatry and Neuroscience of Paris)[20] (C57BL/6J background), as described.[43] In brief, pancreata were minced and digested for 30 minutes at 37°C in a dissociation buffer containing 0.05% collagenase P (Sigma-Aldrich, Lyon, France), 0.1% DNase I (Sigma-Aldrich), and 0.02% Pronase (Sigma-Aldrich) in Grey's balanced salt solution (GBSS; Sigma-Aldrich). Digested pancreata were filtered through a 100-μm nylon mesh and washed in GBSS with 0.3% bovine serum albumin (BSA). After spinning, the cell pellet was resuspended in 12 mL GBSS with 0.3% BSA and 10 mL 43.75% Nicodenz (Sigma-Aldrich). A total of 11 mL cell suspension was layered below 4.5 mL of GBSS with 0.3% BSA, and the gradient was centrifuged for 20 minutes at 2600 rpm (with break switched off). The cells in the fuzzy band just above the interface between the Nicodenz and

---

Figure 6. (*See previous page*). **Macrophage polarization, ECM deposit, and angiogenesis are decreased in primary KPC tumors upon combination treatment as compared with gemcitabine.** Quantification and representative pictures of markers analyzed by immunohistochemistry using the indicated antibodies in KPC primary tumors (Tum.). Each value represents the marker quantification in each tumor (n = 8 mice/group). (*A* and *B*) Phospho-γH2AX–positive cells (in % of total cells). *Scale bars*: 50 μm. (*C–F*) Quantification of (*C*) Ki-67–positive cells (in % of total cells), and of (*D*) CD8-positive cells, (*E*) lymphocyte antigen 6 complex locus G [Ly6G]-positive cells, or (*F*) myeloperoxidase (MPO)-positive cells (number/field). (*G* and *H*) CD206 mean fluorescence intensity (in intensity of each field). *Scale bars*: 100 μm. (*I* and *J*) αSMA-positive area (in % of each total field area). (*K* and *L*) Turquoise blue/green-positive area from Movat pentachrome staining (in % of each total field area). (*M*) Quantification of phospho-STAT3–positive cells (in number/mm^2). (*N*) Representative pictures. (*O*) Quantification of MECA32-positive cells (in % of 4′,6-diamidino-2-phenylindole [DAPI]-positive cells) (n = 4–6 mice/group). (*P*) Quantification of NG2/MECA32 double-positive cells (% of NG2-positive pericytic cells in the Meca32-positive cell population, as in [46] (n = 4–6 mice/group). Kruskal–Wallis test followed by the Dunn multiple comparison post-test was used to generate *P* values. *$P <$ .05, **$P <$ .01. p-STAT3, phospho-signal transducer and activator of transcription.
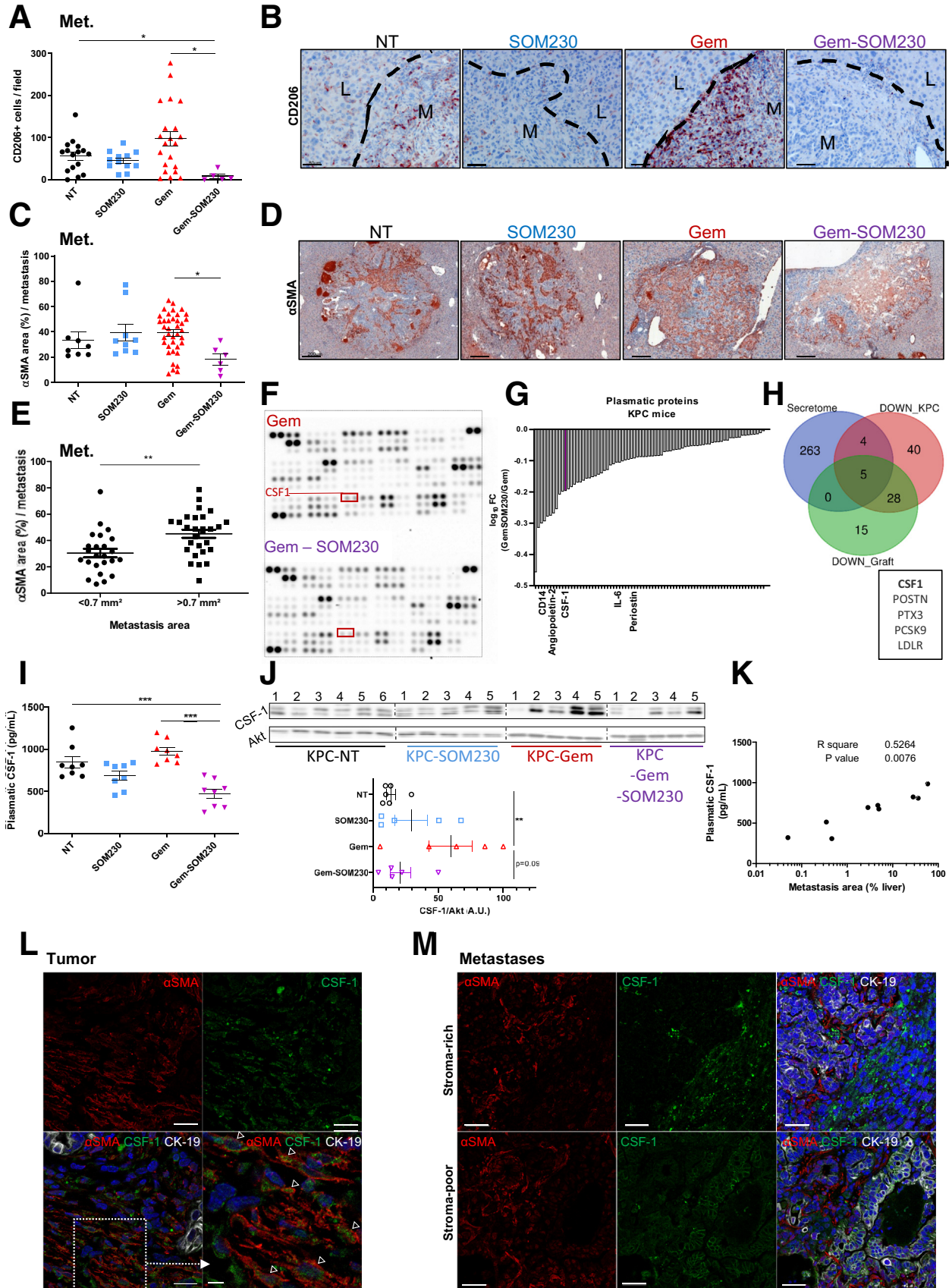
GBSS were harvested, washed in phosphate-buffered saline (PBS), and plated. PSCs were transduced with a lentivector expressing a full-length human CSF-1 (a gift from M. Roussel and C. Sherr, plasmid 86797; Addgene, Watertown, MA).[44] Lentivector pLoc CSF1-181 Ires tGFP Blast was obtained by ligating digested polymerase chain reaction (PCR) product of CSF-1 (AA 1-181) with into BamHI/NheI-digested pLoc-Ires tGFP Blast (Dharmacon, Horizon Discovery LTD, Cambridge UK). CAFs were isolated from human pancreatic tumor tissues by outgrowth, using the explant techniques from histologically fibrotic areas of pancreas surgically resected from PDA patients.[15] Human pancreatic tumor tissues were obtained from the Pathology Department of Limoges Hospital (Limoges, France), from patients undergoing pancreatic resections for pancreatic adenocarcinoma (convention CRB/MAD-CC-2013-002). Small tissue blocks were cut (0.5–1 mm^3) using a razor blade and were seeded in 10 cm^2 uncoated culture wells in the presence of Dulbecco's modified Eagle medium–F12 containing 10% fetal calf de-complemented serum. Tissue blocks were cultured at 37°C in a 5% CO^2–air humidified atmosphere. Eighteen hours after seeding, culture medium was changed. CAFs grew out from the tissue blocks 1–3 days later. An authorization for collecting and conserving this collection was given by the Comité de Protection des Personnes Sud-Ouest et Outre-Mer II (Déclaration de Conservation et Préparation de Collections DC-2016-2654). This study was approved by the Ethic Committee of the Institution.

Secretome Liquid Chromatography MS/MS Analysis

Ten to 15 mL of secretomes from CAFs (from n = 9 tumor patients), treated or not for 48 hours with SOM230 (10^{-7} mol/L), and from CAF culture immortalized with hTERT (human telomerase reverse transcriptase [CAFhTERT]), were analyzed in biological duplicates by nano-liquid chromatography-MS/MS using an Ultimate3000 system (Dionex, ThermoFisher Scientific) coupled to an Orbi-trap Tribrid Fusion mass spectrometer (Thermo Fisher Scientific). To take into account the variabilities arising from secretome biochemical preparation and liquid chromatography MS/MS analyses, normalization across the compared samples was performed by adjusting the medians of the distribution of heavy-labeled protein intensities arising from CAFhTERT (used as an internal standard) for all runs. To do so, a primary CAFhTERT culture was labeled with heavy amino acids (L-arginine and L-lysine) through stable labeling with amino acids in cell culture. Proteins with a fold change of more than 2 and a Student t test P value less than .05 were reported as potentially regulated secreted proteins under SOM230 treatment.

Animal Models

Transgenic mice. KPC, LSL-Kras$^{G12D/+}$; Ink4a$^{fl/fl}$; Pdx-1-Cre$^{+/-}$, and KOsst1 mice have been described previously.[18,20,45]

KPC model. Because the kinetic of tumor onset is heterogeneous in the KPC model,[18] mice were enrolled when 30–200 mm^3 tumor was detected by weekly ultrasound monitoring (Vevo 2100; Fujifilm VisualSonics Amsterdam NL, or Aixplorer; Supersonic Imagine Aix-en-Provence France), as indicated (Figure 5B). Treatments were started at homogeneous tumor sizes (Figure 5C). Mice were treated subcutaneously with SOM230-LAR (80 mg/kg, once every 28 days) and/or intraperitoneally with gemcitabine (100 mg/kg, twice per week). Mouse ages and tumor volumes at treatment start and death (ethical end points) are reported (Table 3, Figure 5B and C). All mice were killed when primary tumor volume reached 1 cm^3, or when mice developed ethical clinical end points (Table 3). Age at death was not statistically different between treatment groups (Table 3), except for untreated mice, which lived for a shorter length of time. Survival events were scored when 1 ethical end

Figure 7. (*See previous page*). **Stroma analyses of KPC metastases, and quantification of tumor and plasmatic CSF-1 expression according to mouse treatment and metastasis size.** (*A–D*) Quantification and representative immunohisto-chemistry pictures of (*A* and *B*) CD206-positive cells (number/field), and of (*C* and *D*) αSMA-positive area (in % of each metastasis area). Each value represents the marker quantification per liver metastasis (n = 6–38 metastases/group). L, liver; M, metastasis. Kruskal–Wallis test followed by the Dunn multiple comparison post-test was used to generate P values. (*E*) Representation of αSMA-positive area (in % of each metastasis area) for each KPC liver metastasis (Met.), and according to metastasis size (<0.7 mm^2 or >0.7 mm^2). The unpaired Student t test was used to generate P values. (*F* and *G*) Cytokine array quantification of plasma proteins in KPC mice treated with the combination (gemcitabine plus SOM230) compared with gemcitabine alone (pool of n = 5 mouse plasma/treatment condition), (*F*) showing the membranes, and (*G*) down-regulated proteins (pool of n = 5 mice/group). (*H*) Venn diagram of the overlap of SOM230 down-regulated plasma proteins from KPC (treatment Gem-SOM230 vs Gem) (Table 4), from grafted mice (Figure 3A and B, Table 2), both identified using cytokine arrays, and from CAF secretome analysis (Figure 1, Table 1). Common proteins are listed in the *right panel*. (*I*) Plasma CSF-1 ELISA quantification in KPC mice treated or not (NT) with gemcitabine (Gem) or SOM230 or gemcitabine + SOM230 (n = 8 mice/treatment condition), at death. Each *dot* represents CSF-1 plasma concentration measured in 1 mouse. Analysis of variance followed by the Bonferroni multiple comparison post-test was used to generate P values. (*J*) Western blot analysis of tumor lysates from KPC mice, treated or not (NT) with gemcitabine (Gem), SOM230, or gemcitabine + SOM230 (n = 5–6 mice/treatment condition, randomly chosen from the n = 8 mice enrolled in each treatment group), with anti–CSF-1 and Akt (loading control) antibody, and underneath, quantification (densitometric analysis) of CSF-1 normalized to Akt expression (A.U., arbitrary unit). Analysis of variance followed by the Bonferroni multiple comparison post-test was used to generate P values. (*K*) Correlation between plasma CSF-1 concentrations and metastasis liver area in KPC mice (untreated mice, n = 12). (*L* and *M*) Immunofluorescence confocal images of αSMA (red), CSF-1 (green), and CK-19 (white) on formalin-fixed, paraffin-embedded tissue slides of (*L*) KPC primary tumors, scale bar: 20 μm (except for the *lower-right panel*, which is a magnification of the *lower-left panel* [*dashed-lined box*], scale bar: 10 μm), and (*M*) in liver metastases, either stroma-rich (3 *upper panels*) or stroma-poor (3 *lower panels*), scale bar: 50 μm. *P < .05, **P < .01, and ***P < .001. IL, interleukin.

Table 4. Listing of Down-Regulated Proteins in KPC Plasma: Gemcitabine-SOM230 Vs Gemcitabine

Protein names	Log ratio Gem-SOM230/Gem
Osteoprotegerin	-0.4554106
WISP-1	-0.3132871
CD14	-0.2991138
Myeloperoxidase	-0.2927159
Serpin F1	-0.2775624
Angiopoietin-2	-0.2744032
CCL21	-0.2670901
Endoglin	-0.2538754
Serpin E1	-0.2071946
MMP-3	-0.1980219
M-CSF	-0.1955245
CCL22	-0.1905704
BAFF	-0.1831733
Adiponectin	-0.1755342
CCL17	-0.1687388
Gas 6	-0.1684436
IL23	-0.1624154
TNF-α	-0.1563117
Proliferin	-0.1550597
LDL R	-0.1511058
IL17A	-0.1482403
C1q R1	-0.1431448
Pref-1	-0.1390524
E-selectin	-0.1310115
IGFBP-3	-0.1281087
VEGF	-0.1134834
CD160	-0.1099336
IL6	-0.1047299
MMP-9	-0.1046919
CXCL13	-0.1005212
IL3	-0.09737246
MMP-2	-0.0957026
Periostin	-0.09313533
PCSK9	-0.09101482
Osteopontin	-0.08783475
IGFBP-5	-0.08713286
CXCL16	-0.08686412
Complement component C5	-0.08671959
CCL6	-0.08508948
CD40	-0.08502961
CXCL1	-0.08414122
CX3CL1	-0.08342186
Pentraxin 3	-0.08190633
IGFBP-2	-0.07113896
RBP4	-0.06947069
IL15	-0.0686098
Thrombopoietin	-0.06512675
TIM-1	-0.06420811
GDF-15	-0.06296449

Table 4. Continued

Protein names	Log ratio Gem-SOM230/Gem
VCAM-1	-0.05980025
IL1β	-0.05504656
CXCL10	-0.05379479
ICAM-1	-0.0524515
Complement factor D	-0.05201
Fetuin A	-0.05186915
FGF-21	-0.05006535
Chitinase 3-like 1	-0.0484128
IL1α	-0.04661465
EGF	-0.04635749
IGFBP-6	-0.04144023
Angiopoietin-like 3	-0.04035782
PD-ECGF	-0.03923278
P-selectin	-0.03810753
Flt-3 ligand	-0.03448458
IL7	-0.03444469
Chemerin	-0.02659499
CCL12	-0.02634445
CXCL9	-0.02562579
Endostatin	-0.02464836
HGF	-0.01868339
IFN-γ	-0.0183519
IL1ra	-0.0171957
DPPIV	-0.01625448
Lipocalin-2	-0.01578041
IGFBP-1	-0.01393292
CXCL11	-0.01046351
CCL11	-0.004502624

NOTE. Pool of n = 5 mice/group.
BAFF, B-cell activating factor; CCL, CC chemokine ligand; CXCL, (C-X-C) motif ligand; DPPIV, dipeptidyl-peptidase IV; EGF, epidermal growth factor; FGF, fibroblast growth factor; Flt-3, fms like tyrosine kinase 3; GDF, glial-derived factor; HGF, hepatocyte growth factor; ICAM-1, intercellular adhesion molecule-1; IFN, interferon; IGFBP, insulin-like growth factor binding-protein; IL, interleukin; LDL, low-density lipoprotein; MMP, matrix metalloproteinase; PCSK9, proprotein convertase subtilisin/kexin type-9; PD-ECGF, platelet-derived endothelial cell growth factor; RBP, retinol binding protein; TIM-1, T cell Ig and Mucin 1; TNF, tumor necrosis factor; VCAM-1, vascular cell adhesion molecule 1; VEGF, vascular endothelial growth factor; WISP, Wnt-1 inducible signaling pathway.

point was reached (tumor burden >1000 mm^3, or body weight loss >20%, or reaching any clinical end point defined by our institutional guidelines and European animal protection law).

Orthotopic graft models. Age-matched 8-week-old female C57BL/6J mice were used (Charles River Laboratories, Ecully France). Syngeneic orthotopic tumors were established by surgical implantation of a 1:3 mix of pancreatic cancer KPC cells (2.10^4) and PSCs (6.10^4). Mice were treated
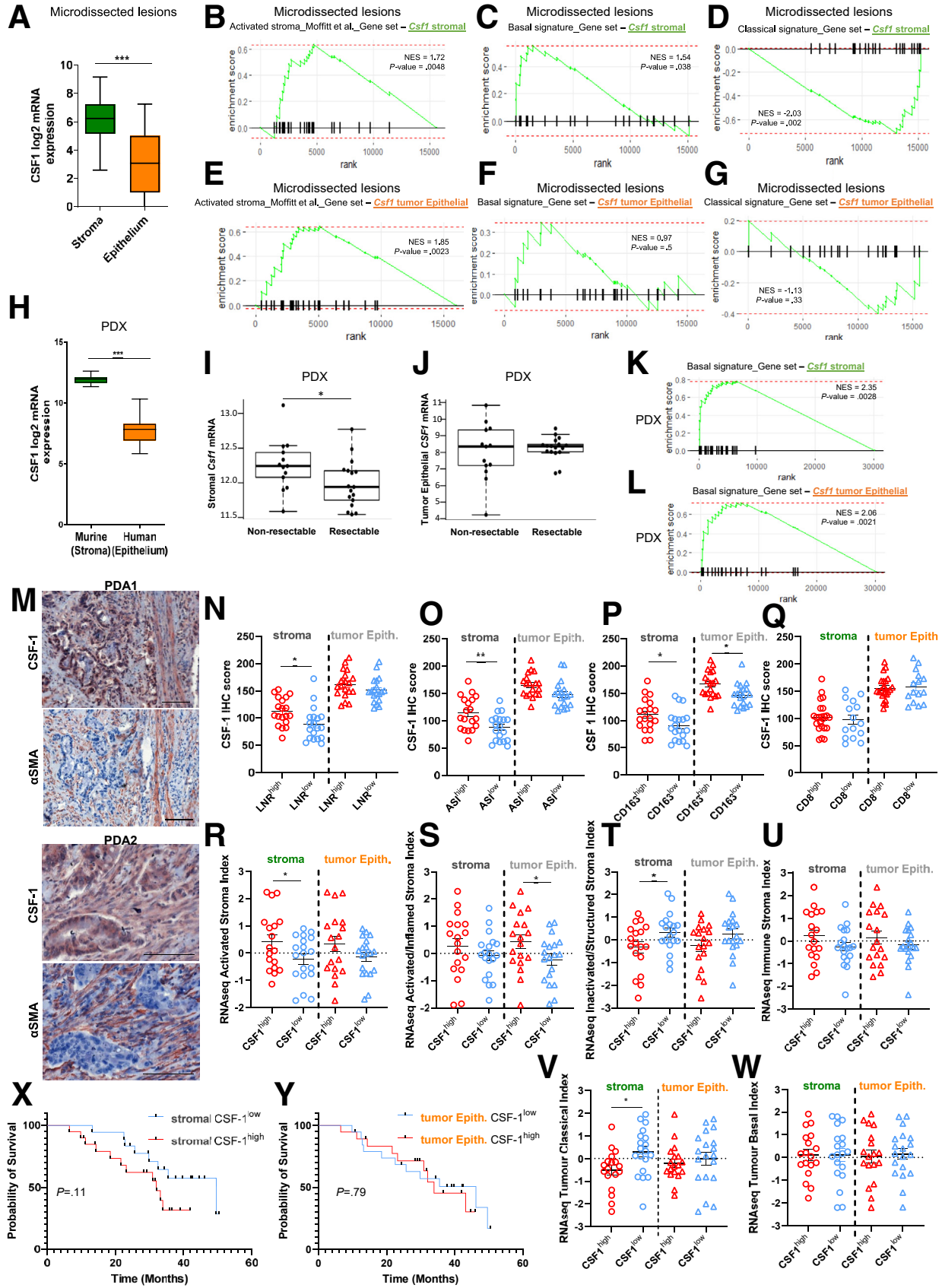
subcutaneously with SOM230-long-acting release (LAR) (80 mg/kg, once every 28 days) and/or intraperitoneally with gemcitabine (100 mg/kg, twice per week) or PBS. SOM230-LAR was provided by Novartis. Gemcitabine was obtained from the Institut Universitaire du Cancer de Toulouse pharmacy and diluted in PBS. Treatments started 3 weeks after grafting when mice were randomly placed in one of the treatment groups (untreated, PBS; and SOM230-LAR–treated). Tumor volumes were measured by ultrasound using the 3-dimensional reconstruction tool (Vevo 2100; VisualSonics), or with the following formula tumor area × tumor diameter × (2/3) (Aixplorer; Supersonic Imagine). For metastasis analysis, formalin-fixed paraffin-embedded lungs or livers were cut (5-μm–thick sections), and 5 slides (every 100 μm) were colored (hematoxylin and eosin) and examined for the presence of metastasis foci. Metastasis foci were identified in each organ section, the corresponding area was quantified, and the metastatic load was calculated as the cumulated area of metastases quantified per section and expressed as the percentage of the total organ area per section, using the NanoZoomer Digital Pathology Virtual Slide Viewer (Hamamatsu Photonics, Massy, France). A cut-off value equal to the calculated median of the cumulative metastatic lung or liver area (percentage of the total organ area) and quantified in the control untreated condition was set to discriminate between mice presenting with a low vs a high metastatic load. All experiments were in accordance with institutional guidelines and European animal protection law and approved by the responsible government agency (agreement number APAFIS21117 2019061900061441).

Colorations and Immunostaining of Mouse Tissues

Formalin-fixed, paraffin-embedded tumor tissue slides were deparaffinized/rehydrated and stained (H&E or Movat's pentachrome). For immunostaining, slides subjected to antigen retrieval (10 mmol/L sodium citrate pH 6, or Tris-EDTA pH 8.8 and autoclaved), quenched for peroxidase activity, and blocked using blocking buffer (X0909; Dako, Agilent Technologies, Les Ulis, France). Slides were incubated with the following primary antibodies overnight at 4°C: anti-αSMA (ab7817, 1/200; Abcam, Amsterdam, NL), anti–CSF-1 (ab99178, 1/200; Abcam), anti–lymphocyte antigen 6 complex locus G (RB6-8C5, ab25377, 1/100; Abcam), antimyeloperoxidase (ab188211, 1/500; Abcam), anti–phospho-STAT3 (Tyr705, D3A7, CST9145, 1/200; Cell Signaling Technology, Danvers, MA), anti-Ki-67 (SP6, ab16667, 1/200; Abcam), anti–phospho-γH2AX (Ser139, 20E3, CST9718, 1/500; Signaling Technology), anti-CD8 (D4W2Z, CST98941, 1/400; Signaling Technology), anti-sst1 (a generous gift from Novartis Pharma, now commercialized by Bio-Rad (Marnes la Coquette, France) MCA5924, dilution 1/250). Slides were washed and incubated in ImmPRESS secondary antibody (mouse MP-7402, rabbit MP7401, or rat MP7404; Vector), and binding was visualized with 3,3'-diaminobenzidine substrate kit (SK4105; Vector, Eurobio Scientific, Les Ulis, France) or aminoethyl carbazole substrate chromogen (K3464; Dako), and counterstained with hematoxylin. Sections were imaged using Nano-Zoomer XR (Hamamatsu) (service provided by Imag'IN core from the Institut Universitaire du Cancer Toulouse). Quantifications were performed using ImageJ (National

Figure 8. (*See previous page*). **Stromal CSF-1 is a factor of poor prognosis in human PDA.** (*A–G*) Analyses of stromal and of tumor epithelial CSF-1 mRNA expression in correlation with functional molecular signatures of PDA stroma and tumor cells, in the Maurer et al[27] data set (RNAseq analyses of laser-microdissected PDA lesions [n = 65 tumors] of the tumor epithelium [tumor Epith.] and of the stroma). (*A*) Differential expression of CSF-1 mRNA in laser-microdissected PDA lesions of the stroma or of the tumor epithelium (tumor Epith.) (n = 65 tumors) from Maurer et al.[27] The unpaired *t* test with Welch correction was used to generate *P* values. (*B and E*) GSEA for activated stromal signature, as defined by Moffitt et al,[4] or for (*C and F*) epithelial cancer basal-like signature, or for (*D and G*) epithelial cancer classic-like signature, in (*B–D*) high vs low stromal or (*E–G*) tumor epithelial CSF-1 mRNA-expressing lesions from Maurer et al.[27] (*H–L*) Analyses of stromal and tumor epithelial CSF-1 mRNA expression in correlation with functional molecular signatures of PDA stroma and tumor cells, in the Nicolle et al data set (PaCaOmics, n = 30 PDX).[5] (*H*) Differential expression of CSF-1 mRNA in stromal (of murine origin) or tumor epithelial (of human origin) cells. The unpaired *t* test with Welch correction was used to generate *P* values. (*I and J*) Correlation between (*I*) stromal or (*J*) tumor epithelial level of CSF-1 mRNA with resectability of patients. The Mann–Whitney test was used to generate *P* values. (*K and L*) GSEA for pancreatic cancer cell basal signature in high vs low (*K*) stromal or (*L*) tumor epithelial CSF-1 mRNA PDX. (*M–Y*) Analyses of stromal and of tumor epithelial CSF-1 protein expression, in correlation with clinical data of patients, with pathologic data of PDA tumors, and with functional molecular signatures of PDA stroma and tumor cells (RNAseq analyses), in a personal PDA cohort (n = 38 primary tumors). (*M*) Representative images of CSF-1 and αSMA expression analyzed by immunohistochemistry on formalin-fixed, paraffin-embedded tissue slides of 2 PDA patient primary tumors (PDA1 and PDA2). (*N–W*) Quantification using Definiens Tissue Studio of CSF-1 immunohistochemistry (IHC) scores in the stromal (*left panels*) or in the tumor epithelial (*right panels*) compartment, and (*N*) plotted in correlation with a high vs low (based on the median) positive lymph node ratio (LNR), (*O*) with pathologic markers of the tumors quantified by IHC, that is, activated stroma index (ASI), (*P*) CD163-positive cells, or (*Q*) CD8-positive cells. (*R–W*) RNAseq analyses of the n = 38 PDA tumors generated transcriptomic signature index, as defined by[6], of the (*R*) activated stroma index, (*S*) activated/inflamed stroma index, (*T*) inactivated/structured stroma index, and (*U*) immune stroma index, and of the tumor epithelium, (*V*) classic-like index or (*W*) basal-like index, which were compared in CSF-1^{high} vs CSF-1^{low} (based on the median) IHC scores quantified in the stroma (*left panel*) or in the tumor epithelium (*right panel*). The unpaired *t* test was used to generate *P* values. (*X and Y*) Survival analysis of patients presenting a (*X*) high vs low stromal or (*Y*) tumor epithelial CSF-1 immunohistochemistry score. Kaplan–Meier survival data were analyzed using a log-rank test. *$P < .05$, **$P < .01$, and ***$P < .001$

Table 5. Links Between Stromal or Tumor Epithelial High Vs Low CSF-1 mRNA Quantified in Microdissected Lesions From the Maurer et al[27] Patient Cohort (n = 65), With Clinical Features of Patient Disease

	Stroma				Tumoral		
	CSF-1 high	CSF-1 low	P		CSF-1 high	CSF-1 low	P
Age, mean, y (minimum–maximum)	68.4 (48–86)	69.6 (50–85)	.614	Age, mean, y (minimum–maximum)	67.4 (48–86)	70.6 (48–86)	**.047**
AJCC stage			**.0358**	AJCC stage			.2664
2A	5	12		2A	10	7	
2B	28	17		2B	20	25	
3	0	2		3	1	0	
4	0	1		4	0	2	
Surgical margins			.8281	Surgical margins			.2812
Negative	25	24		Negative	21	28	
Positive	8	8		Positive	10	6	
Race			.7332	Race			.4392
Asian	0	1		Asian	1	0	
Black	2	1		Black	2	1	
Hispanic Latino	1	1		Hispanic Latino	0	2	
Other	1	1		Other	2	0	
White	25	27		White	23	29	
White Latino	1	1		White Latino	1	1	
White non-Hispanic	1	0		White non-Hispanic	1	0	
Unknown	2	0		Unknown	2	0	
Sex			.1701	Sex			.7221
Female	19	12		Female	16	15	
Male	14	20		Male	15	19	
Location			.2935	Location			.2249
Body	0	3		Body	0	3	
Body tail	1	0		Body tail	0	1	
Diffuse	0	1		Diffuse	0	1	
Head	27	24		Head	26	25	
Head body	1	0		Head body	0	1	
Neck	0	1		Neck	0	1	
Tail				Tail	5	2	
Tumor grade			.5944	Tumor grade			.0819
Moderate	18	12		Moderate	12	18	
Moderate to poor	8	8		Moderate to poor	10	6	
Poor	4	6		Poor	4	6	
Well	2	3		Well	1	4	
Well to moderate	1	3		Well to moderate	4	0	
Histology			.9876	Histology			.9629
Ductal Adenocarcinoma	33	31		Ductal adenocarcinoma	30	34	
IPMN carcinoma	0	1		IPMN carcinoma	1	0	
Solid pattern			.6973	Solid pattern			**.0428**
Yes	30	29		Yes	31	28	
No	3	3		No	0	6	
Mucinous features			.9782	Mucinous features			.2057
Yes	32	30		Yes	28	34	
No	1	2		No	3	0	
Clear cell features			.6487	Clear cell features			.4867
Yes	56	6		Yes	28	31	
No	3	0		No	3	3	
Micropapillary growth			.9507	Micropapillary growth			.9144
Yes	54	6		Yes	28	32	
No	5	0		No	3	2	
Features of possible concomitant IPMN			.8399	Features of possible concomitant IPMN			.3521
Yes	52	6		Yes	26	32	
No	7	0		No	5	2	

Table 5. Continued

	Stroma				Tumoral		
	CSF-1 high	CSF-1 low	*P*		CSF-1 high	CSF-1 low	*P*
Stroma subtype			<u>.0769</u>	Tumoral subtype			.6025
ECM-rich	12	16		Basal-like	9	13	
Immune-rich	17	8		Classic	22	21	
NA	4	8					

NOTE. Clinical variables were compared in CSF-1 high vs CSF-1 low groups (comprising tumors with higher or lower CSF-1 mRNA expression than the median, respectively), both in the stroma and in the tumor epithelial compartments, using the unpaired *t* test or the chi-squared test for continuous or categoric variables, respectively. Underline indicates *P* < .1. Boldface indicates *P* < .05.
AJCC, American Joint Committee on Cancer; IPMN, Intraductal Papillary Mucinous Neoplasm.

Institutes of Health, Bethesda, MD) or Qupath software (opensource software for digital pathology image) (5 fields per mouse, at least 5 mice per group, as indicated in the figure legends).

For immunofluorescence staining, the following antibodies were used: anti–mannose receptor (anti-CD206, ab64693, 1/500; Abcam), anti-cytokeratin-19 (conjugated to Alexa Fluor 647, ab192980, 1/100; Abcam), and anti-αSMA, anti-sst1, and anti–CSF-1 as for immunohistochemistry, and then in 4′,6-diamidino-2-phenylindole (1/1000, D9545; Sigma-Aldrich), plus secondary antibodies goat anti-mouse Alexa Fluor 488 (1/1000, A-11001; Invitrogen, ThermoFisher Scientific) or goat anti-rabbit Alexa Fluor 647 (1/1000, A-21244; Invitrogen). Slides were mounted in fluorescent mounting medium (S3023; Dako), and images were acquired using a Cell Observer Videomicroscope (Zeiss) or a confocal microscope (LSM 780; Carl Zeiss Microscopy, Marly Le Roi, France). Quantification was performed using ImageJ software on multiple tissue sections (5 fields per mouse, at least 5 mice per group, as indicated in the figure legends).

Blood Vessel Density and Pericyte Coverage

Tumor sections were co-immunostained by anti-MECA32 for detecting tumor vessels and anti-nueron glial 2 (NG2) antibodies for staining pericytes. Tumor vessels and pericyte coverage analysis were performed as described by Gilles et al.[46] Briefly, tumor blood vessel density and pericyte coverage were plotted as the percentage of the MECA32 staining normalized to nuclei or the percentage of the co-localization between MECA32 and NG2 normalized to nuclei. Immunofluorescence images of tumor sections of PDA were captured by using a FV1000 IX81 laser-scanning confocal microscope (Olympus, Thorlabs, Maisons-Laffitte, France), with a 10× or 40× oil objective. Acquisitions were performed with the same settings on multiple tissue sections (5 fields per mouse, at least 5 mice per group, as indicated in the figure legends) and included negative controls for determination of background staining, which was negligible.

Flow-Cytometric Analysis

Single-cell suspensions were prepared (Tumor Dissociation Kit, 130-096-730, Miltenyi Biotec, Paris, France) and incubated with fluorophore-conjugated anti-mouse antibodies (CD45 [30-F11], CD3 [17-A2], CD4 [RM4-5], CD8 [53-6.7], CD11b [M1/70], Ly-6g [1A8]; all from BD Biosciences, Le Pont de Claix, France), CD206 (C068C2) (from BioLegend EU Amsterdam, NL), and F4/80 (BM8; from ThermoFisher Scientific). Data acquisition was performed on the Fortessa LSR (BD Biosciences) and BD FacsDiva software was used for analysis, as published previously.[47]

Western Blot

Cell lysis was performed in lysis buffer (20 mmol/L Tris, pH 7.5, 150 mmol/L NaCl, 1 mmol/L EDTA, 1% NP40, 1 mmol/L sodium orthovanadate, 1 mmol/L sodium fluoride, and a cocktail of protease inhibitors; Roche (Basel, Switzerland), and tumors were crushed with the Precellys device (Ozyme, Saint Cyr l'Ecole, France) in lysis buffer. The protein extract concentration was measured using the Protein Assay reagent (Bio-Rad). Equal amounts of proteins were resolved by sodium dodecyl sulfate–polyacrylamide gel electrophoresis and electroblotted onto nitrocellulose membranes. Membranes were blocked (5% powdered milk in Tris-buffered saline with 0.1% Tween 20) followed by incubation with primary antibodies (anti–CSF-1 [ab99178, dilution 1/1000] and anti-sst1 antibody [ab2366, dilution 1/1000] from Abcam; anti-Akt [CST9272, dilution 1/1000] and anti-phospho-Akt [p473-Akt, CST2013, dilution 1/1000] from Cell Signalling Technologies; anti–β-actin [A5441, dilution 1/1000] is from Millipore (Merck, Fontenay-sous-Bois, France); and anti-periostin [sc 67233, dilution 1/200] from Santa Cruz (SCBT, Dallas, TX). Membranes were incubated with horseradish-peroxidase–coupled secondary antibody and treated with Pierce ECL Western Blotting Substrate (ThermoFisher Scientific) before detection with the PXi imaging system (Syngene, Cambridge, UK). SUnSET assay, a nonradioactive equivalent of 35S-Met assay based on puromycin incorporation into nascent polypeptides, was used to monitor the rate of protein synthesis using an

antipuromycin antibody (12D10, dilution 1/1000; Merck Millipore).[21]

ELISA and Cytokine Arrays

CSF-1 detection in plasma was performed using the Mouse Macrophage CSF Quantikine ELISA Kit (MMC00; R&D Systems, Minneapolis, MN) according to the manufacturer's instructions. Cytokine detection in patient CAF culture supernatant was performed using ELISA kits (macrophage-CSF, DMC00B; connective tissue growth factor, DY9190-05; THSB2 (thrombospondin-2), DTSP20; all from R&D Systems, and biglycan ab245709; Abcam), according to the manufacturer's instructions. Cytokine assay was performed using the Proteome Profiler Mouse XL Cytokine Array Kit (ARY028; R&D Systems) according to the manufacturer's instructions. Membrane chemiluminescences were captured with the PXi imaging system (Syngene, Cambridge, UK)). Data acquisition and quantification was performed using Quick Spots Tool software (Western Vision Software, Salt Lake City, UT).

Quantitative Real-Time PCR

Total RNA from PSCs and spleen was isolated using TRIzol (ThermoFisher Scientific). Reverse-transcription quantitative PCR reactions were performed using RevertAid H Minus Reverse Transcriptase (ThermoFisher Scientific) and SoFast EvaGreen Supermix (Bio-Rad) according to the manufacturer's instructions and measured with the StepOne Real-Time PCR Systems (ThermoFisher Scientific). Relative quantitation values were normalized using the comparative Ct (cycle threshold) method. Primers for mouse SSTR1 (somatostatin receptor subtype 1) were as follows: forward: 5'-TGCCCTTTCTGGTCACTTCC-3', reverse: 5'-AGCGGTCCACACTAAGCACA-3', and for mouse housekeeping RPS16 (40S ribosomal protein S16) were as follows: forward: 5'-AATGGGCTCATCAAGGTGAACGGA-3', reverse: 5'-TATCCACACCAGCAAATCGCTCCT-3'.

Patient Pancreatic Cancer Tissues for Immunohistochemistry and RNAseq Analyses

Thirty-eight consecutive patients were selected from a retrospective cohort of patients with localized (non-metastatic) PDA who underwent complete surgical resection between December 2011 and January 2014 at Beaujon University Hospital (Clichy, France; Biobank registration number BB-0033-00078).[22] All participants provided their informed consent before taking part. Exclusion criteria were as follows: neoadjuvant chemotherapy and/or radiotherapy, macroscopically incomplete resection (R2), tumor histology other than PDA, and insufficient tumor material available for research. Clinical and pathologic variables were collected retrospectively, including sex, age at diagnosis, tumor site, preoperative assessment of tumor extension, surgical procedure, resection margins (R0, negative; R1, positive), differentiation grade, tumor size, tumor stage, lymph node status (negative, N-; positive, N+), LNR (ie, the ratio of lymph nodes with tumor metastasis to the total lymph nodes analyzed), TNM classification, and the presence of vascular and perineural invasion. The outcome variable was overall survival, defined as the time interval between the day of surgical resection and death (all causes) or date of last follow-up evaluation, at which point data were censored. Survival curves were estimated using the Kaplan–Meier method and compared using the log-rank test. For immunohistochemistry analyses, whole formalin-fixed paraffin-embedded (FFPE) slides were stained with each indicated antibody, after manual selection by a specialist pancreatic pathologist (J.C.) of tumoral areas on scanned slides. For αSMA (M0851; Dako) and pan-cytokeratin (MSK098-05; Zytomed, Berlin, Germany), the Precision image analysis software (Aperio, Leica Biosystems, Nanterre, France) was used for automated biomarker quantification. The activated stroma index was adapted from Erkan et al[28] by considering the following formula: 1 – pan-cytokeratin-stained area, as a surrogate for the collagen deposit area and calculated using the following formula: αSMA-stained surface/(1 – pan-cytokeratin-stained surface). Anti-CD8–stained (M710301; Dako) and anti-CD163–stained (NCL-CD163; Leica) tumor slides were assessed visually by 2 observers (J.C. and C.N.), to score according to the localization (peritumoral or intratumoral) and frequency of respective positive cell aggregates (low score, no intratumoral aggregate with possible low frequency of peritumoral aggregates; high score, low or high frequency of intratumoral aggregates with possible high frequency of peritumoral aggregates). For CSF-1 stain quantification in stromal or tumoral areas, the calculated CSF-1 immunohistochemistry score takes into account the stain intensity and the percentage of the stained cell area. Percentages of cells expressing low, medium, and high CSF-1 stain were quantified using Definiens Tissue Studio (Imag'IN core Institut Universitaire du Cancer, Toulouse, France) in stromal or tumor compartments, as we published previously,[47] and a CSF-1 score was calculated as follows: $1 \times$ % low CSF-1 cells $+ 2 \times$ % medium CSF-1 cells $+ 3 \times$ % high CSF-1 cells. Associations between the activated stroma index, CD163, or CD8 scores (high vs low, ie, higher than or less than the median, respectively), and CSF-1 immunohistochemistry scores in the stroma or in the tumor were assessed using unpaired Student t tests.

For RNAseq analyses, FFPE blocks were selected by a specialist pancreatic pathologist (J.C.). The presence of neoplastic cells was confirmed and tumor-enriched zones after examination of H&E–stained slides were macrodissected for nucleic acid extraction. For all samples, RNA was extracted using the Qiagen RNeasy FFPE kit following the manufacturer's instructions (Qiagen, Hilden, Germanyia). A total of 150 ng RNA was used as starting material for the preparation of RNAseq libraries using the QuantSeq 3' REV kit (Lexogen, Vienna, Austria). Libraries were sequenced on an Illumina (San Diego, CA) NovaSeq platform aiming for 7Millions read pairs.

Bioinformatics

For secretome analysis, GSEA was performed using the fast GSEA implementation (10.18129/B9.bioc.fgsea;

Bioconductor, open source software), using the matrix of the measurable proteins identified in CAF conditioned media (n = 9) preranked by the significance of the differential test (untreated vs SOM230-treated condition). Therefore, secretome GSEA results show enrichments, induced by SOM230, among the proteins identified in CAF conditioned media. PDX transcriptome analyses were obtained from the processed data set of the PaCaOmics clinical trial (NCT01692873).[5] Laser-microdissected stromal and epithelial compartments of RNAseq analyses from 65 PDA patients were obtained from the gene omnibus database (GSE93326).[27] Patient clinical data were available and correlation with stromal and tumoral CSF-1 mRNA expression was assessed. The transcriptomic data set from the Beaujon cohort RNAseq analyses on PDA FFPE tissues (n = 38 patients) was characterized according to the 6 robust transcriptomic components of the tumor and of the stroma, identified by independent component analysis in a published cohort of 309 PDA patients[6] (ie, tumoral basal, tumoral classic, stromal activated, stromal inflammatory, stromal structured vascularized, and stromal immune), assigning a weight of each component to each FFPE sample. Associations between CSF-1 immunohistochemistry scores in the stroma or in the tumor (high vs low) and transcriptomic components were assessed using unpaired Student t tests.

Statistics

All statistical analyses were performed using GraphPad Prism 6 software (GraphPad Software, Inc, San Diego, CA). The number of animals and replicate in vitro experiments are specified in each figure legend. Results are presented as the means ± SEM. The Kaplan–Meier method was used to estimate survival rates, and significance was determined by the log-rank test. Normal distribution of variables was computed using the D'Agostino–Pearson normality test. Comparison of a continuous variable in 2 groups or more than 2 groups with normal distribution was performed using the parametric test (ie, t test or analysis of variance, respectively), and with a Bonferroni post-test for multiparametric analyses. If the variable was not distributed normally, a nonparametric test (ie, Mann–Whitney or Kruskal–Wallis), was applied for comparison in 2 or more groups, respectively, with a Dunn post-test for multiparametric analyses. The significance of metastasis frequency was determined by the Fisher exact test. All P values were 2-sided, and $P < .05$ was considered statistically significant.

All authors had access to the study data and reviewed and approved the final manuscript.

References

1. Kleeff J, Korc M, Apte M, La Vecchia C, Johnson CD, Biankin AV, Neale RE, Tempero M, Tuveson DA, Hruban RH, Neoptolemos JP. Pancreatic cancer. Nat Rev Dis Primers 2016;2:16022.
2. Collisson EA, Sadanandam A, Olson P, Gibb WJ, Truitt M, Gu S, Cooc J, Weinkle J, Kim GE, Jakkula L, Feiler HS, Ko AH, Olshen AB, Danenberg KL, Tempero MA, Spellman PT, Hanahan D, Gray JW. Subtypes of pancreatic ductal adenocarcinoma and their differing responses to therapy. Nat Med 2011; 17:500–503.
3. Bailey P, Chang DK, Nones K, Johns AL, Patch AM, Gingras MC, Miller DK, Christ AN, Bruxner TJ, Quinn MC, Nourse C, Murtaugh LC, Harliwong I, Idrisoglu S, Manning S, Nourbakhsh E, Wani S, Fink L, Holmes O, Chin V, Anderson MJ, Kazakoff S, Leonard C, Newell F, Waddell N, Wood S, Xu Q, Wilson PJ, Cloonan N, Kassahn KS, Taylor D, Quek K, Robertson A, Pantano L, Mincarelli L, Sanchez LN, Evers L, Wu J, Pinese M, Cowley MJ, Jones MD, Colvin EK, Nagrial AM, Humphrey ES, Chantrill LA, Mawson A, Humphris J, Chou A, Pajic M, Scarlett CJ, Pinho AV, Giry-Laterriere M, Rooman I, Samra JS, Kench JG, Lovell JA, Merrett ND, Toon CW, Epari K, Nguyen NQ, Barbour A, Zeps N, Moran-Jones K, Jamieson NB, Graham JS, Duthie F, Oien K, Hair J, Grutzmann R, Maitra A, Iacobuzio-Donahue CA, Wolfgang CL, Morgan RA, Lawlor RT, Corbo V, Bassi C, Rusev B, Capelli P, Salvia R, Tortora G, Mukhopadhyay D, Petersen GM, Australian Pancreatic Cancer Genome I, Munzy DM, Fisher WE, Karim SA, Eshleman JR, Hruban RH, Pilarsky C, Morton JP, Sansom OJ, Scarpa A, Musgrove EA, Bailey UM, Hofmann O, Sutherland RL, Wheeler DA, Gill AJ, Gibbs RA, Pearson JV, Waddell N, Biankin AV, Grimmond SM. Genomic analyses identify molecular subtypes of pancreatic cancer. Nature 2016; 531:47–52.
4. Moffitt RA, Marayati R, Flate EL, Volmar KE, Loeza SG, Hoadley KA, Rashid NU, Williams LA, Eaton SC, Chung AH, Smyla JK, Anderson JM, Kim HJ, Bentrem DJ, Talamonti MS, Iacobuzio-Donahue CA, Hollingsworth MA, Yeh JJ. Virtual microdissection identifies distinct tumor- and stroma-specific subtypes of pancreatic ductal adenocarcinoma. Nat Genet 2015; 47:1168–1178.
5. Nicolle R, Blum Y, Marisa L, Loncle C, Gayet O, Moutardier V, Turrini O, Giovannini M, Bian B, Bigonnet M, Rubis M, Elarouci N, Armenoult L, Ayadi M, Duconseil P, Gasmi M, Ouaissi M, Maignan A, Lomberk G, Boher JM, Ewald J, Bories E, Garnier J, Goncalves A, Poizat F, Raoul JL, Secq V, Garcia S, Grandval P, Barraud-Blanc M, Norguet E, Gilabert M, Delpero JR, Roques J, Calvo E, Guillaumond F, Vasseur S, Urrutia R, de Reynies A, Dusetti N, Iovanna J. Pancreatic adenocarcinoma therapeutic targets revealed by tumor-stroma cross-talk analyses in patient-derived xenografts. Cell Rep 2017;21:2458–2470.
6. Puleo F, Nicolle R, Blum Y, Cros J, Marisa L, Demetter P, Quertinmont E, Svrcek M, Elarouci N, Iovanna J, Franchimont D, Verset L, Galdon MG, Deviere J, de Reynies A, Laurent-Puig P, Van Laethem JL, Bachet JB, Marechal R. Stratification of pancreatic ductal adenocarcinomas based on tumor and microenvironment features. Gastroenterology 2018;155:1999–2013.e3.
7. Vennin C, Murphy KJ, Morton JP, Cox TR, Pajic M, Timpson P. Reshaping the tumor stroma for treatment of pancreatic cancer. Gastroenterology 2018;154:820–838.

8. Kalluri R. The biology and function of fibroblasts in cancer. Nat Rev Cancer 2016;16:582–598.

9. Knudsen ES, Vail P, Balaji U, Ngo H, Botros IW, Makarov V, Riaz N, Balachandran V, Leach S, Thompson DM, Chan TA, Witkiewicz AK. Stratification of pancreatic ductal adenocarcinoma: combinatorial genetic, stromal, and immunologic markers. Clin Cancer Res 2017;23:4429–4440.

10. Kitamura T, Qian BZ, Pollard JW. Immune cell promotion of metastasis. Nat Rev Immunol 2015;15:73–86.

11. Candido JB, Morton JP, Bailey P, Campbell AD, Karim SA, Jamieson T, Lapienyte L, Gopinathan A, Clark W, McGhee EJ, Wang J, Escorcio-Correia M, Zollinger R, Roshani R, Drew L, Rishi L, Arkell R, Evans TRJ, Nixon C, Jodrell DI, Wilkinson RW, Biankin AV, Barry ST, Balkwill FR, Sansom OJ. CSF1R(+) macrophages sustain pancreatic tumor growth through T cell suppression and maintenance of key gene programs that define the squamous subtype. Cell Rep 2018; 23:1448–1460.

12. Zhang A, Qian Y, Ye Z, Chen H, Xie H, Zhou L, Shen Y, Zheng S. Cancer-associated fibroblasts promote M2 polarization of macrophages in pancreatic ductal adenocarcinoma. Cancer Med 2017;6:463–470.

13. Helms E, Onate MK, Sherman MH. Fibroblast heterogeneity in the pancreatic tumor microenvironment. Cancer Discov 2020;10:648–656.

14. Neesse A, Bauer CA, Ohlund D, Lauth M, Buchholz M, Michl P, Tuveson DA, Gress TM. Stromal biology and therapy in pancreatic cancer: ready for clinical translation? Gut 2019;68:159–171.

15. Duluc C, Moatassim-Billah S, Chalabi-Dchar M, Perraud A, Samain R, Breibach F, Gayral M, Cordelier P, Delisle MB, Bousquet-Dubouch MP, Tomasini R, Schmid H, Mathonnet M, Pyronnet S, Martineau Y, Bousquet C. Pharmacological targeting of the protein synthesis mTOR/4E-BP1 pathway in cancer-associated fibroblasts abrogates pancreatic tumour chemoresistance. EMBO Mol Med 2015;7:735–753.

16. Moatassim-Billah S, Duluc C, Samain R, Jean C, Perraud A, Decaup E, Cassant-Sourdy S, Bakri Y, Selves J, Schmid H, Martineau Y, Mathonnet M, Pyronnet S, Bousquet C. Anti-metastatic potential of somatostatin analog SOM230: indirect pharmacological targeting of pancreatic cancer-associated fibroblasts. Oncotarget 2016;7:41584–41598.

17. Wiley SZ, Sriram K, Liang W, Chang SE, French R, McCann T, Sicklick J, Nishihara H, Lowy AM, Insel PA. GPR68, a proton-sensing GPCR, mediates interaction of cancer-associated fibroblasts and cancer cells. FASEB J 2018;32:1170–1183.

18. Hingorani SR, Wang L, Multani AS, Combs C, Deramaudt TB, Hruban RH, Rustgi AK, Chang S, Tuveson DA. Trp53R172H and KrasG12D cooperate to promote chromosomal instability and widely metastatic pancreatic ductal adenocarcinoma in mice. Cancer Cell 2005;7:469–483.

19. Principe DR, Narbutis M, Kumar S, Park A, Viswakarma N, Dorman MJ, Kamath SD, Grippo PJ, Fishel ML, Hwang RF, Thummuri D, Underwood PW, Munshi HG, Trevino JG, Rana A. Long-term gemcitabine treatment reshapes the pancreatic tumor microenvironment and sensitizes murine carcinoma to combination immunotherapy. Cancer Res 2020; 80:3101–3115.

20. Videau C, Hochgeschwender U, Kreienkamp HJ, Brennan MB, Viollet C, Richter D, Epelbaum J. Characterisation of [125I]-Tyr0DTrp8-somatostatin binding in sst1- to sst4- and SRIF-gene-invalidated mouse brain. Naunyn Schmiedebergs Arch Pharmacol 2003; 367:562–571.

21. Schmidt EK, Clavarino G, Ceppi M, Pierre P. SUnSET, a nonradioactive method to monitor protein synthesis. Nat Methods 2009;6:275–277.

22. Neuzillet C, Tijeras-Raballand A, Ragulan C, Cros J, Patil Y, Martinet M, Erkan M, Kleeff J, Wilson J, Apte M, Tosolini M, Wilson AS, Delvecchio FR, Bousquet C, Paradis V, Hammel P, Sadanandam A, Kocher HM. Inter- and intra-tumoural heterogeneity in cancer-associated fibroblasts of human pancreatic ductal adenocarcinoma. J Pathol 2019;248:51–65.

23. Yagiz K, Rittling SR. Both cell-surface and secreted CSF-1 expressed by tumor cells metastatic to bone can contribute to osteoclast activation. Exp Cell Res 2009; 315:2442–2452.

24. DeNardo DG, Ruffell B. Macrophages as regulators of tumour immunity and immunotherapy. Nat Rev Immunol 2019;19:369–382.

25. Laklai H, Miroshnikova YA, Pickup MW, Collisson EA, Kim GE, Barrett AS, Hill RC, Lakins JN, Schlaepfer DD, Mouw JK, LeBleu VS, Roy N, Novitskiy SV, Johansen JS, Poli V, Kalluri R, Iacobuzio-Donahue CA, Wood LD, Hebrok M, Hansen K, Moses HL, Weaver VM. Genotype tunes pancreatic ductal adenocarcinoma tissue tension to induce matricellular fibrosis and tumor progression. Nat Med 2016;22:497–505.

26. Keskin D, Kim J, Cooke VG, Wu CC, Sugimoto H, Gu C, De Palma M, Kalluri R, LeBleu VS. Targeting vascular pericytes in hypoxic tumors increases lung metastasis via angiopoietin-2. Cell Rep 2015;10:1066–1081.

27. Maurer C, Holmstrom SR, He J, Laise P, Su T, Ahmed A, Hibshoosh H, Chabot JA, Oberstein PE, Sepulveda AR, Genkinger JM, Zhang J, Iuga AC, Bansal M, Califano A, Olive KP. Experimental microdissection enables functional harmonisation of pancreatic cancer subtypes. Gut 2019;68:1034–1043.

28. Erkan M, Michalski CW, Rieder S, Reiser-Erkan C, Abiatari I, Kolb A, Giese NA, Esposito I, Friess H, Kleeff J. The activated stroma index is a novel and independent prognostic marker in pancreatic ductal adenocarcinoma. Clin Gastroenterol Hepatol 2008;6:1155–1161.

29. Catenacci DV, Junttila MR, Karrison T, Bahary N, Horiba MN, Nattam SR, Marsh R, Wallace J, Kozloff M, Rajdev L, Cohen D, Wade J, Sleckman B, Lenz HJ, Stiff P, Kumar P, Xu P, Henderson L, Takebe N, Salgia R, Wang X, Stadler WM, de Sauvage FJ, Kindler HL. Randomized phase Ib/II study of gemcitabine plus placebo or vismodegib, a hedgehog pathway inhibitor, in patients with metastatic pancreatic cancer. J Clin Oncol 2015; 33:4284–4292.

30. Hakim N, Patel R, Devoe C, Saif MW. Why HALO 301 failed and implications for treatment of pancreatic cancer. Pancreas (Fairfax) 2019;3:e1–e4.

31. Suleiman Y, Mahipal A, Shibata D, Siegel EM, Jump H, Fulp WJ, Springett GM, Kim R. Phase I study of combination of pasireotide LAR + gemcitabine in locally advanced or metastatic pancreatic cancer. Cancer Chemother Pharmacol 2015;76:481–487.

32. Miller BW, Morton JP, Pinese M, Saturno G, Jamieson NB, McGhee E, Timpson P, Leach J, McGarry L, Shanks E, Bailey P, Chang D, Oien K, Karim S, Au A, Steele C, Carter CR, McKay C, Anderson K, Evans TR, Marais R, Springer C, Biankin A, Erler JT, Sansom OJ. Targeting the LOX/hypoxia axis reverses many of the features that make pancreatic cancer deadly: inhibition of LOX abrogates metastasis and enhances drug efficacy. EMBO Mol Med 2015; 7:1063–1076.

33. Takeuchi S, Baghdadi M, Tsuchikawa T, Wada H, Nakamura T, Abe H, Nakanishi S, Usui Y, Higuchi K, Takahashi M, Inoko K, Sato S, Takano H, Shichinohe T, Seino K, Hirano S. Chemotherapy-derived inflammatory responses accelerate the formation of immunosuppressive myeloid cells in the tissue microenvironment of human pancreatic cancer. Cancer Res 2015;75:2629–2640.

34. Karagiannis GS, Condeelis JS, Oktay MH. Chemotherapy-induced metastasis: molecular mechanisms, clinical manifestations, therapeutic interventions. Cancer Res 2019;79:4567–4576.

35. Pothula SP, Xu Z, Goldstein D, Biankin AV, Pirola RC, Wilson JS, Apte MV. Hepatocyte growth factor inhibition: a novel therapeutic approach in pancreatic cancer. Br J Cancer 2016;114:269–280.

36. Bonelli S, Geeraerts X, Bolli E, Keirsse J, Kiss M, Pombo Antunes AR, Van Damme H, De Vlaminck K, Movahedi K, Laoui D, Raes G, Van Ginderachter JA. Beyond the M-CSF receptor - novel therapeutic targets in tumor-associated macrophages. FEBS J 2018;285:777–787.

37. Mroczko B, Szmitkowski M, Wereszczynska-Siemiatkowska U, Jurkowska G. Hematopoietic cytokines in the sera of patients with pancreatic cancer. Clin Chem Lab Med 2005;43:146–150.

38. Kuen J, Darowski D, Kluge T, Majety M. Pancreatic cancer cell/fibroblast co-culture induces M2 like macrophages that influence therapeutic response in a 3D model. PLoS One 2017;12:e0182039.

39. Mitchem JB, Brennan DJ, Knolhoff BL, Belt BA, Zhu Y, Sanford DE, Belaygorod L, Carpenter D, Collins L, Piwnica-Worms D, Hewitt S, Udupi GM, Gallagher WM, Wegner C, West BL, Wang-Gillam A, Goedegebuure P, Linehan DC, DeNardo DG. Targeting tumor-infiltrating macrophages decreases tumor-initiating cells, relieves immunosuppression, and improves chemotherapeutic responses. Cancer Res 2013;73:1128–1141.

40. Zhu Y, Knolhoff BL, Meyer MA, Nywening TM, West BL, Luo J, Wang-Gillam A, Goedegebuure SP, Linehan DC, DeNardo DG. CSF1/CSF1R blockade reprograms tumor-infiltrating macrophages and improves response to T-cell checkpoint immunotherapy in pancreatic cancer models. Cancer Res 2014;74:5057–5069.

41. Steins A, van Mackelenbergh MG, van der Zalm AP, Klaassen R, Serrels B, Goris SG, Kocher HM, Waasdorp C, de Jong JH, Tekin C, Besselink MG, Busch OR, van de Vijver MJ, Verheij J, Dijk F, van Tienhoven G, Wilmink JW, Medema JP, van Laarhoven HW, Bijlsma MF. High-grade mesenchymal pancreatic ductal adenocarcinoma drives stromal deactivation through CSF-1. EMBO Rep 2020;21:e48780.

42. Davidson S, Efremova M, Riedel A, Mahata B, Pramanik J, Huuhtanen J, Kar G, Vento-Tormo R, Hagai T, Chen X, Haniffa MA, Shields JD, Teichmann SA. Single-cell RNA sequencing reveals a dynamic stromal niche that supports tumor growth. Cell Rep 2020; 31:107628.

43. Vonlaufen A, Phillips PA, Yang L, Xu Z, Fiala-Beer E, Zhang X, Pirola RC, Wilson JS, Apte MV. Isolation of quiescent human pancreatic stellate cells: a promising in vitro tool for studies of human pancreatic stellate cell biology. Pancreatology 2010;10:434–443.

44. Roussel MF, Dull TJ, Rettenmier CW, Ralph P, Ullrich A, Sherr CJ. Transforming potential of the c-fms proto-oncogene (CSF-1 receptor). Nature 1987;325:549–552.

45. Aguirre AJ, Bardeesy N, Sinha M, Lopez L, Tuveson DA, Horner J, Redston MS, DePinho RA. Activated Kras and Ink4a/Arf deficiency cooperate to produce metastatic pancreatic ductal adenocarcinoma. Genes Dev 2003; 17:3112–3126.

46. Gilles ME, Maione F, Cossutta M, Carpentier G, Caruana L, Di Maria S, Houppe C, Destouches D, Shchors K, Prochasson C, Mongelard F, Lamba S, Bardelli A, Bouvet P, Couvelard A, Courty J, Giraudo E, Cascone I. Nucleolin targeting impairs the progression of pancreatic cancer and promotes the normalization of tumor vasculature. Cancer Res 2016; 76:7181–7193.

47. Zaghdoudi S, Decaup E, Belhabib I, Samain R, Cassant-Sourdy S, Rochotte J, Brunel A, Schlaepfer D, Cros J, Neuzillet C, Strehaiano M, Alard A, Tomasini R, Rajeeve V, Perraud A, Mathonnet M, Pearce OM, Martineau Y, Pyronnet S, Bousquet C, Jean C. FAK activity in cancer-associated fibroblasts is a prognostic marker and a druggable key metastatic player in pancreatic cancer. EMBO Mol Med 2020;12:e12010.

Correspondence
Address correspondence to: Corinne Bousquet, VMD, PhD, INSERM U1037, Cancer Research Center of Toulouse, 2 Avenue Hubert Curien, CS53717, 31037 Toulouse Cedex 1, France. e-mail: corinne.bousquet@inserm.fr; fax: (33) (0) 56131-9752.

CRediT Authorship Contributions

Rémi Samain, PharmD, PhD (Conceptualization: Supporting; Formal analysis: Equal; Investigation: Equal; Methodology: Equal; Writing – original draft: Supporting; Writing – review & editing: Supporting)

Alexia Brunel, MS (Formal analysis: Supporting; Investigation: Supporting; Methodology: Supporting)

Thibault Douché, MS (Investigation: Supporting; Methodology: Supporting)

Marjorie Fanjul, PhD (Methodology: Supporting)

Julia Rochotte, PhD (Formal analysis: Supporting; Investigation: Supporting; Methodology: Supporting)

Stéphanie Cassant-Sourdy, Tech (Investigation: Supporting)

Jérôme Cros, MD, PhD (Investigation: Supporting; Resources: Lead)

Cindy Neuzillet, MD, PhD (Investigation: Supporting; Methodology: Supporting)

Jérôme Raffenne, PhD (Investigation: Supporting; Methodology: Supporting)

Camille Duluc, PhD (Investigation: Supporting; Methodology: Supporting)

Aurélie Perraud, PhD (Methodology: Supporting)

Jérémy Nigri, PhD (Methodology: Supporting)

Véronique Gigoux, PhD (Methodology: Supporting)

Ivan Bieche, PhD (Methodology: Supporting)

Mattéo Ponzo, MS (Methodology: Supporting)

Gilles Carpentier, PhD (Methodology: Supporting)

Ilaria Cascone, PhD (Investigation: Supporting; Methodology: Supporting)

Richard Tomasini, PhD (Investigation: Supporting; Methodology: Supporting)

Herbert A Schmid, PhD (Conceptualization: Supporting; Funding acquisition: Supporting)

Muriel Mathonnet, MD, PhD (Resources: Supporting)

Rémy Nicolle, PhD (Conceptualization: Supporting; Investigation: Supporting; Methodology: Supporting; Writing – review & editing: Supporting)

Marie-Pierre Bousquet, PhD (Conceptualization: Supporting; Investigation: Equal; Methodology: Supporting; Supervision: Supporting; Writing – review & editing: Supporting)

Yvan Martineau, PhD (Conceptualization: Supporting; Funding acquisition: Supporting; Investigation: Supporting; Methodology: Supporting; Supervision: Supporting; Writing – review & editing: Supporting)

Stéphane Pyronnet, PhD (Conceptualization: Supporting; Funding acquisition: Equal; Supervision: Supporting; Writing – review & editing: Supporting)

Christine Jean, PhD (Conceptualization: Supporting; Formal analysis: Supporting; Funding acquisition: Supporting; Investigation: Supporting; Methodology: Supporting; Supervision: Equal; Writing – review & editing: Supporting)

Corinne Bousquet, VMD, PhD (Conceptualization: Lead; Formal analysis: Lead; Funding acquisition: Lead; Investigation: Supporting; Methodology: Supporting; Project administration: Lead; Supervision: Lead; Validation: Lead; Writing – original draft: Lead)

Conflicts of interest

The authors disclose no conflicts.